U–Pb detrital zircon dates and source provenance analysis of Phanerozoic sequences of the Congo Basin, central Gondwana

Bastien Linol, Maarten J. de Wit, Erika Barton, Michiel C.J. de Wit, François Guillocheau

***Graphical Abstract (for review)**

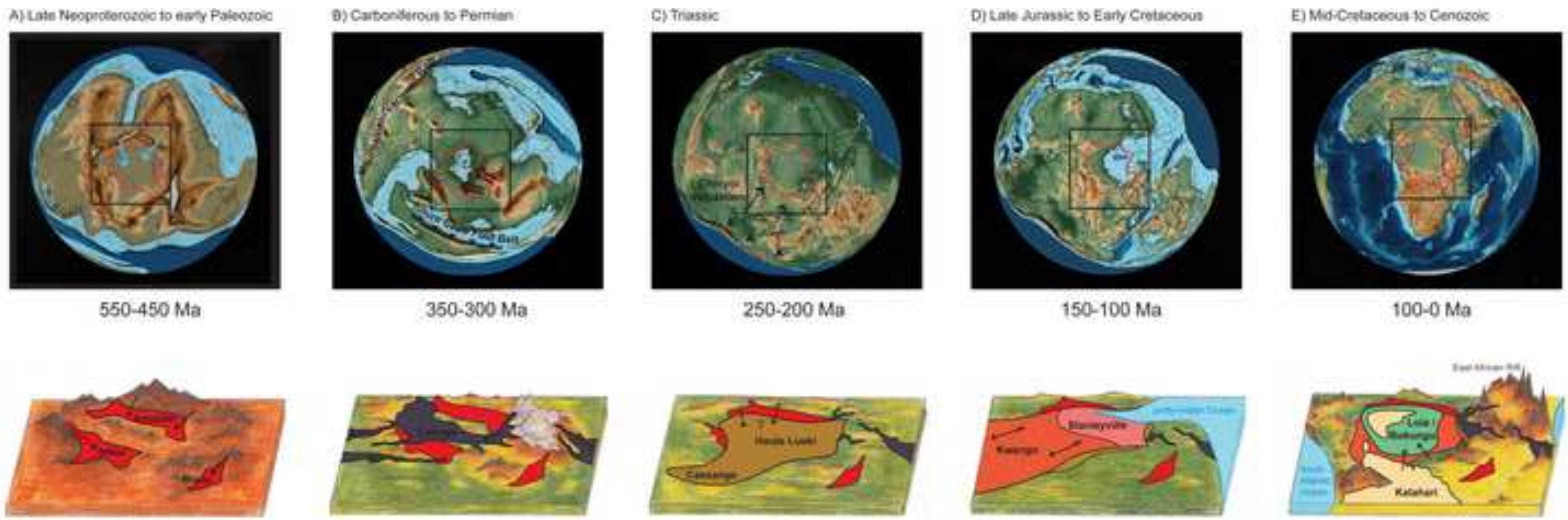

*Highlights (for review)

- A revised stratigraphy for one of the least-known large continental basins
- Track the evolution of central Gondwana via U-Pb detrital zircon geochronology
- Early Neoproterozoic (1 Ga) dates dominated in all samples

U-Pb detrital zircons dates and source provenance analysis of Phanerozoic sequences of the Congo Basin, central Gondwana

Bastien Linol[1,2], Maarten J. de Wit[1], Erika Barton[1,2], Michiel (Mike) J.C. de Wit[3] and Francois Guillocheau[4]

[1] AEON-ESSRI (African Earth Observatory Network – Earth Stewardship Science Research Institute.

[2] Department of Geoscience, Nelson Mandela Metropolitan University, Port Elizabeth, South Africa.

Corresponding author: bastien.aeon@gmail.com

[3] Delrand Resources Pty Ltd., Toronto, Ontario, Canada.

[3] Geosciences, University of Rennes1, France.

Abstract

The Congo Basin (CB) is the largest sediment sink of central Gondwana, built on a mosaic of Precambrian crustal blocks amalgamated during the mid-Paleoproterozoic (Eburnian; 2.1-1.8 Ga), late Mesoproterozoic (Kibaran; 1.4-1.0 Ga), and late Neoproterozoic-early Cambrian (Pan African; 750-500 Ma). Sporadic uplift, tilting and erosion of these Precambrian terrains form the source regions for the sedimentary sequences that fill the CB. We investigate the Phanerozoic successions in the field and along four historic deep boreholes drilled in the center of the basin, and date detrital zircons from the main stratigraphic groups to characterize their provenance ages and reconstruct the paleogeographic evolution of the CB during amalgamation and break-up of the Gondwana supercontinent. Sedimentological data show that the oldest, upper Neoproterozoic-lower Paleozoic Redbeds (the Inkisi, Aruwimi and Biano Groups) were derived from the north. Zircons from these sequences have two dominant age-populations of 1100-950 Ma and 800-600 Ma, likely sourced from Kibaran and Pan African terrains within the Oubanguides (e.g. the Central Saharan Belt) and parts of the North African Shield (e.g. Darfour). The overlying Carboniferous-Permian glacial and deglaciation sequences (the Lukuga Group) have similar peaks, as well as abundant zircons of 2.05-1.85 Ga and a subordinate number dated at 1.42-1.37 Ga. The latter are from Eburnian and Kibaran sources in east-central Africa, consistent with west-facing glacial paleo-valleys preserved along the

eastern margin of the CB. The succeeding Triassic (the Haute-Lueki Group) and Jurassic-Cretaceous (the Kwango Group) fluvial and aeolian red sandstones were again derived from the north. Their range of zircon dates also has two main peaks at 1000 Ma and 600 Ma, but also contain small younger grains of 290-240 Ma and 200-190 Ma. We interpret these younger zircons to be derived from volcanic dust that originated during late Paleozoic-Jurassic magmatism of the Choiyoi and Chon Aike Provinces flanking the Andean subduction margin of Gondwana. By contrast, the uppermost Cenozoic alluviums of the CB (the Kalahari Group) contain diamond concentrates and large zircon fragments dated at 3-2.5 Ga, derived from the Kasai and Cuango Cratons, to the south, which host Cretaceous diamondiferous kimberlites.

Keywords: Phanerozoic, Congo Basin, detrital zircons, sediment provenances, central Gondwana.

1. Introduction

The Congo Basin (CB) is a large (ca. 1.8 million km^2) Phanerozoic sedimentary basin near the center of Africa (Fig. 1) whose origin and tectonic evolution are poorly understood, mostly because of a lack of modern chronostratigraphy (Kadima et al., 2011; Sachse et al., 2012; Linol, 2013; Linol et al., 2014a, and b; de Wit and Linol, 2014). The CB was initially explored during the 1940s and 1950s, when that region, now the Democratic Republic of Congo (DRC), was part of the Belgian Congo. This early work included extensive field mapping (e.g. Robert, 1946; Cahen, 1954; Lepersonne, 1974), geophysical surveys (e.g. Jones et al., 1959; Evrard, 1960), and the drilling and coring of two deep boreholes (each ca. 2 km deep), named Samba and Dekese (Cahen et al., 1959, and 1960). These holes represent unique stratigraphic sections through the center of the basin and are now archived at the Royal Museum for Central Africa (RMCA) in Tervuren (Belgium). In the 1970s, after independence, petroleum exploration companies acquired new seismic reflection data along 36 profiles, and drilled two more (non-cored) deep boreholes, the Gilson-1 and Mbandaka-1 wells (each more than 4 km deep; EssoZaire, 1981a, and b; Lawrence and Makazu, 1988; Daly et al., 1991, and 1992). This data was used to define the geometry of main stratigraphic sequences and revealed in subsurface a series of northwest-southeast trending basement highs near the center of the basin. These highs were interpreted to have formed as a result of far-field tectonic stresses during Neoproterozoic and late Paleozoic collision processes along Gondwana's paleo-Pacific margins (Daly et al., 1991, and 1992; Trouw and de Wit, 1999). Since these two exploration programs, very little new stratigraphic data has been acquired across the CB, hampering regional correlations and modern interpretation of its geodynamic history (Giresse, 2005; Crosby et al., 2010; Kadima et al., 2011; Buiter et al., 2012; Linol et al., 2014c).

Here, we present new U-Pb detrital zircon dates from outcrops along the Kwango River in southwestern DRC, and from selected core samples of the Samba and Dekese sections. Together with improved field, seismic and borehole stratigraphic correlations, sediment dispersal directions, and a review of dated basement rocks in and around central Africa (and central Gondwana), this source provenance analysis attempts to retrace the paleogeographic evolution of the CB during the Phanerozoic, from the time of final assembly to the break-up of the Gondwana supercontinent. Although the regional extent (one field study and two boreholes sites) and number of samples (9 samples) are limited, these U-Pb results are among the first detrital zircon dates for the CB, providing new information on the geodynamic history of interior Gondwana.

2. Geological setting

The CB is completely surrounded by Precambrian rocks, including several Archean cratonic blocks (i.e. cratons) and Proterozoic belts with regionally distinct geologic and thermo-tectonic histories, together referred to as the Central African Shield (de Wit et al., 2008; de Wit and Linol, 2014; Fig. 1A). This shield amalgamated with others continental fragments (e.g. the Kalahari and North African Shields) during the late Neoproterozoic to early Cambrian Pan African orogens (750-500 Ma; Fritz et al., 2013) to form central Gondwana, thereafter making up the foundation (i.e. crystalline basement) and providing sediments to the Phanerozoic CB (Fig. 1B).
[Figure 1 here]

Precambrian basement

The Central African Shield comprises the Kasai, NE Angola (Cuango), Ntem, Mboumou and Tanzanian Cratons (ca. 3.5-2.5 Ga; Cahen et al., 1984), surrounding the CB (Fig. 1A). These blocks amalgamated with mid-Paleoproterozoic terrains along the Ruwenzori and Ubendian-Usagaran Belts (ca. 2.1-1.8 Ga) in Uganda and western Tanzania (Lenoir et al., 1995; Link et al., 2010; Boniface et al., 2012), the Central Angolan Mobile Belt (CAMB; ca. 2.3-2.0 Ga) in Angola (de Carvalho et al., 2000; de Wit and Linol, 2014), and the West Central African Mobile Belt (WCAMB; ca. 2.5-2.0 Ga) in western DRC, Gabon and Cameroon (Caen-Vachette et al., 1988; Feybesse et al., 1998), that extends to Transamazonian terrains in northeastern Brazil (e.g. Toteu et al., 2001; Lerouge et al., 2006; Pedrosa-Soares et al., 2008). This assemblage was subsequently affected by mid-Mesoproterozoic granitoid magmatism along the Kibaran Belt in eastern DRC, Rwanda and Burundi (ca. 1.4 Ga; Tack et al., 2010; Fernandez-Alonso et al., 2012), and again deformed during the late Mesoproterozoic to early Neoproterozoic (ca. 1 Ga) within the Oubanguides in the Central African Republic (CAR) and Chad (e.g. the Central Saharan Belt; de Wit et al., 2014), and along the Irumide-Mozambique Belts in Zambia and northern Mozambique (Jamal, 2005; de Waele et al., 2008; Bingen et al., 2009; Roberts et al., 2012).

A Central African Shield was then finally consolidated during the Pan African along a vast system of peripheral mobile belts, folded-and-thrusted concentrically toward the proto-CB. This includes: the ca. 700-500 Ma West Congo Belt (de Carvalho et al., 2000; Tack et al., 2001; Frimmel et al., 2006; Monié et al., 2012): the Oubanguides (ca. 850-550 Ma; Poidevin, 1985; Rolin, 1995; Toteu et al., 2006; Nkoumbou et al., 2013); the Mozambique Belt (ca. 700-550 Ma; Sommer et al., 2003; de Waele et al., 2006; Fritz et al., 2013); and the Lufilian Arc (ca. 750-550 Ma; Kampunzu and Cailteux, 1999) in southeastern DRC and northern Zambia that extends to the southwest in northern Botswana and Namibia (de Wit, 2009; Rankin et al., 2013). All these Pan African mobile belts link to a northeast- and southwest-verging thrust, or “flower structure” (the Kiri High; Daly et al., 1991, and 1992), inferred to exist beneath the center of the CB (Fig. 1A).

Phanerozoic cover of the Central African Shield

The CB preserves five main depositional successions (or “supersequences”; Linol, 2013, see also Linol et al., 2014d) ranging in age from late Neoproterozoic to Cenozoic, with a total thickness of 4-6 km near the center of the basin (Fig. 2).

[Figure 2 here]

The oldest succession, uppermost part of the Neoproterozoic to lower Paleozoic West Congo, Lindi and Katanga Supergroups (Lepersonne, 1974; Poidevin, 1985; Tack et al., 2001; Kanda et al., 2011; Tait et al., 2011), comprises about 1-1.5 km thick Redbeds, deposited regionally southward unconformably across deformed Precambrian carbonate and siliclastic platforms that are exposed around the margins of the CB (Fig. 1B). This includes: the Aruwimi Group that outcrops abundantly south of the Oubanguides; the Inkisi Group, east of the West Congo Belt (Alvarez et al., 1995); and the Biano Group to the north of the Lufilian Arc (Master et al., 2005). Their stratigraphy is relatively poorly constrained by field observations and geochronology, and only detrital zircons dated at 540 Ma provide a maximum early Cambrian age (Jelsma et al., 2011). Equivalent subsurface sequences of red quartzites have been proven only in the Gilson-1 and Dekese wells (Units G10 and D10; Fig. 2) in the south-central part of the basin.

A major erosion surface across the Redbeds represents a hiatus of up to 150 million years. This unconformity is overlain by Carboniferous-Permian and Triassic successions, in total between 1 km and 3 km thick, which represent the northern extensions of the Karoo Supergroup of southern Africa (e.g. Johnson et al., 1996; Catuneanu et al., 2005; Linol et al., 2014a). The lowermost parts, the Lukuga Group, are glacial and deglaciation sequences of diamictite and black shale, and sandstones with thin coal beds, dated by paleobotany from mid-Carboniferous to Late Permian (Boulouard and Calandra, 1963; Bose and Kar, 1978; Colin and Jan du Chêne, 1981). The Lukuga Group is best preserved in east-west-trending paleo-valleys along the eastern margin of the CB (Jamotte, 1932; Boutakoff, 1948; Cahen and Lepersonne, 1978; Fig. 1B), and extends in subsurface to the south-central and western parts of the basin (ca. 900 m thick at Dekese; Fig. 2). The overlying Triassic Haute Lueki Group is less precisely described in outcrop (Lombard, 1961; Bose and Kar 1976; Cahen, 1981) but, most likely is laterally equivalent to widespread arid fluvial-aeolian sequences (also “red-beds”) in south-central Africa, such as for example the Cassange Group in Angola (Antunes et al., 1990), the Lebung Group in Botswana (Bordy et al., 2010), the Omingonde Formation in Namibia (Miller, 2008), the Beaufort and Stormberg Groups in South Africa (Johnson et al., 1996; Tankard et al., 2012), and in eastern Brazil (e.g. the Santa Maria Group; Zerfass et al., 2004; Milani et al., 2007). It is between 500 m and 1800 m thick in the center of the CB (ca. 900 m at Samba; Fig. 2).

Above these sequences, and overlying a pronounced unconformity that coincides in time with the onset of break-up of Gondwana (ca. 200-160 Ma; Reeves, 1999; Jokat et al., 2003; Torsvik et al., 2012), are Upper Jurassic to Upper Cretaceous sequences of red sandstones, between 500 m and 1000 m thick, which cover the entire CB (Fig. 1B). At the base, the fluvial-deltaic Stanleyville Group intercalates in its lower part with a fossiliferous marine limestone horizon ("Lime Fine"; Cahen, 1983a) that implies a short Kimmeridgian transgression of the proto-Indian Ocean in the northeastern CB (Saint-Seine, 1955; Saint-Seine and Casier, 1962; Taverne, 1975; Giresse, 2005; Linol, 2014b). It is onlapped to the south by northeasterly-derived aeolian dunes of the Lower Kwango Group (Units D4 and G4; Fig. 2), extending continuously to the southwestern margin of the basin (Fig. 3A), and into the Paraná Basin of eastern Brazil (see Linol, 2013, and Linol et al., 2014d for details). In the center of the CB, the succeeding Loia and Bokungu Groups correspond to two superimposed lacustrine sequences (in total ca. 650 m thick at Samba; Fig. 2), both dated biostratigraphically to be Albian-Cenomanian in age (Marlière, 1950; Cox, 1960; Defrétin-Lefranc, 1967; Grékoff, 1957; Maheshwari et al., 1977; Colin, 1981; Cahen, 1983b). These sequences are overlain in the west-central part of the basin by Upper Cretaceous (also fossiliferous) fluvial red sandstones and mudstones of the Upper Kwango Group (Lepersonne, 1951; Saint Seine 1953; Grékoff, 1960; Casier, 1965; Taverne, 1976; Colin, 1994; Linol et al., 2014b).

[Figure 3 here]

The Jurassic-Cretaceous succession of the CB is in turn truncated by a peneplanation surface, covered by silcretes ("Polymorph Sandstones"; c.f. Lepersonne 1951) and alluviums of the Cenozoic Kalahari Group (Leriche, 1927; Polinard, 1932; Grékoff, 1958; de Ploey et al., 1968; Colin, 1994; e.g. Fig. 3B). This youngest sequence is between 40 m and 240 m thick in the center of the basin (Fig. 2).

3. Material and methods

Detrital zircons from nine samples, collected in the field (Fig. 3) and from the Samba and Dekese cores (Fig. 2), were U-Pb dated by Laser Ablation Multi-Collector Inductively Coupled Plasma Mass Spectrometry (LA-MC-ICP-MS; e.g. Cocherie and Robert, 2008). Together with the new sequence-stratigraphic correlations and sediment dispersal directions described above, this geochronology helps understanding the evolution of source provenance ages and associated major geological changes during development of the Phanerozoic CB (e.g. Fedo et al., 2003).

Core samples and preparation

Sampling was done during fieldwork in the Kwango region of the southwest CB, and while logging the Samba and Dekese sections archived at the Royal Museum for Central Africa (RMCA) in Tervuren (Belgium). Two samples from outcrops and seven samples from the two core-sections were analyzed (Figs. 2 and 3), representing 10 kg and 50 kg of red sandstones and gravels, and between 1 m and 5 m of bisected core (1.5-3.5 kg each), respectively.

Heavy minerals were concentrated in the field using an Amstrong-Jig, and in laboratory with the application of heavy liquid (Lithium-based Tungstate) and a Frantz isodynamic separator, at the University of Cape Town (South Africa) and the University of Heidelberg (Germany). The concentrates were examined under the binocular microscope and for each sample between 150 and 200 zircons with different size, shape, color and abundance were carefully hand-picked. Selected grains (e.g. Fig. 4) were then mounted into epoxy disks, abraded down to the center of grains and polished. The mounts were imaged using a JEOL microprobe in both cathodoluminescence and backscatter electron modes to further characterize the internal composition and structure of the zircons (e.g. zoning, inherited cores, overgrowths, recrystallization and fractures). These images are also used to guide the laser to specific sites during U-Pb dating (e.g. Fig. 5).

[Figure 4 here]

Analytical method of dating

U-Pb dating was performed in the AEON EarthLab, using a Nu Plasma HR multi-collector inductively coupled plasma mass spectrometer (Nu Instruments) coupled to a UP 193 solid-state laser system (New Wave Research) and a desolvation nebulizer system (DSN-100, Nu Instruments). The Nu Plasma MC-ICP-MS is equipped with a special collector block allowing for simultaneous detection of ion signals from masses ^{238}U to ^{203}Tl. U and Tl isotopes are measured on Faraday cups, while Pb isotopes are measured on ion counters. For more details see Biggin et al. (2011), and for the general analytical routine Simonetti et al. (2005).

U and Pb data was collected in time-resolved mode including 20 s of instrument background, 20 s of gas and acid blank, and 35 s of sample ablation. The laser was operated at a repetition rate of 10 Hz and an energy density of 2-3 J/cm^2. The spot size varied from 15 µm to 35 µm depending on the size and on the Pb concentration of the analyzed zircon. Raw data were corrected from background signals. Mass bias correction of the ^{207}Pb/^{206}Pb ratio was done using the Tl-doping method of Belshaw et al. (1998). Laser-induced inter-element fractionation and time-dependent Pb/U fractionation of the ^{206}Pb/^{238}U ratio was corrected by standard bracketing of 10 unknowns, with the reference material represented by a fragment of the 611 Ma GJ1 zircon standard with an U concentration of ~ 450 ppm. ^{207}Pb/^{235}U was calculated using ^{207}Pb/^{235}U = ^{207}Pb/^{206}Pb × ^{206}Pb/^{238}U × 137.88. Reported uncertainties were propagated by quadratic addition of the external reproducibility of the standard during the individual analytical session and the internal error of the respective analysis. Reported dates in this study are not common Pb corrected, since correction by the ^{204}Pb method cannot be applied due to the isobaric interference of ^{204}Hg, which is a contaminant of the He gas carrying the ablated material from the laser cell to the MC-ICP-MS. The accuracy of the data was checked by regular analyses of internal standards: from the Kaap Valley pluton (3227 ± 1 Ma; Kamo and Davis, 1994), and the Plešovice zircon standard (337.13 ± 0.37 Ma; Sláma et al., 2008). Concordia plots and probability diagrams were constructed using Isoplot 3.0 (Ludwig, 2003).

4. Results

In total, 568 detrital zircons were analyzed from the different stratigraphic groups (Fig. 5). The U-Pb data for each sample (between 60 and 80 analyses) are presented in Tables 1 to 9. Below, we discuss only ^{206}Pb/^{207}Pb dates that are concordant in the range of 90-110%, unless otherwise mentioned (for the grains younger than 500 Ma).

[Figure 5 here]

[Tables 1 to 9 about here]

Sample D1853 (the Inkisi Group)

63 analyses were performed on 60 grains in samples D1853 (Table 1) from red quartzitic sandstones of the Inkisi Group in the lower part of the Dekese section (Fig. 2). Zircons from this sample are relatively small, sub-rounded and brownish in color (Fig. 4A).

42 single zircon dates are concordant (in the range of 90-110%). The four oldest date between 2671 ±5 Ma and 2575 ±9 Ma. Two zircons date at 2.0 Ga (2041 ±7 Ma and 2036 ±10 Ma), 22 date between 1107 ±12 Ma and 881 ±20 Ma (52%) that represent the most abundant age-population, and 14 date between 835 ±8 Ma and 609 ±21 Ma (33%). Following this distribution, the probability plot shows peaks at 2670 Ma, 2060 Ma, 1040 Ma and 650 Ma (Fig. 5A).

Samples D1400 and D1595 (the Lukuga Group)

In samples D1400 and D1595, from diamictites of the Lukuga Group in the middle part of the Dekese section (Fig. 2), 157 analyses were performed on 148 grains (Tables 2 and 3). Zircons from this group are small to large (200-500 µm), sub-rounded and generally transparent (Fig. 4B).

In total 123 single zircon dates are concordant. The oldest zircon dates at 2925 ±8 Ma. Six zircons date between 2690 ±16 Ma and 2428 ±16 Ma, one dates at 2.2 Ga (2184 ±16 Ma), and 41 date between 2074 ±20 Ma and 1802 ±12 Ma (31%) that represent the most abundant age-population in the samples. Seven zircons date between 1589 ±28 Ma and 1371 ±18 Ma, 40 are between 1235 ±9 Ma and 964 ±20 Ma (30%), and 27 date between 865 ±25 Ma and 544 ±21 Ma (20%). The probability plot shows three distinct peaks at 1930 Ma, 1040 Ma and 680 Ma (Fig. 5B).

Samples S1605 and S2035 (the Haute Lueki Group)

In samples S1605 and S2035, from red quartzitic sandstones of the Haute Lueki Group in the lower part of the Samba section (Fig. 2), 124 analyses were performed on 105 grains (Tables 4 and 5). Zircons from these samples are relatively small, elongated and transparent or brownish in color (Fig. 4C); some have xenotime overgrowths.

In total 56 single zircon dates are concordant. Many zircons are systematically discordant due to common lead loss in the samples. The oldest zircon dates at 2470 ±10 Ma; no Archean dates were found. Four zircons date between 2103 ±5 Ma and 1952 ±11 Ma, 20 date between 1094 ±10 Ma and 899 ±6 Ma (36%), and 31 date between 794 ±16 Ma and 579 ±14 Ma (55%) representing the most abundant age-population. The probability plot shows two major peaks at 1000 Ma and 670 Ma (Fig. 5C).

Samples D470, D600 and WP19 (the Lower Kwango Group)

In samples D470, D600 and WP19, from aeolian red sandstones of the Lower Kwango Group, zircons are generally medium in size, well sorted, well rounded and often transparent (Fig. 4D). Few are small, yellowish and with crystal shapes.

148 analyses were performed on 137 grains in samples D470 and D600 from the upper part of the Dekese section (Tables 6 and 7). In total 94 single zircon dates are concordant in these two samples. The seven oldest zircons date between 2630 ±16 Ma and 2473 ±16 Ma, one dates at 2.1 Ga (2154 ±16 Ma), and eight date between 2080 ±17 Ma and 1788 ±22 Ma (8%). One zircon dates at 1.5 Ga (1548 ±13 Ma), 27 date between 1272 ±23 Ma and 884 ±19 Ma (29%), and 49 date between 837 ±21 Ma and 513 ±21 Ma (52%) that represent the most abundant age-population (Fig. 5D). Following this distribution, the probability plot shows four peaks at 2580 Ma, 2000 Ma, 970 Ma and 680 Ma. The two youngest zircons have $^{206}Pb/^{238}U$ dates of 286 ±7 Ma and 240 ±6 Ma, concordant at 89% and 99%, respectively (Table 6).

In sample WP19, from Kwango red sandstones outcropping at a cliff near Swamasangu (Fig. 3A), 66 analyses were performed on 64 grains (Table 8). 54 single zircon dates are concordant. The oldest zircon dates at 3133 ±29 Ma, four date at 2.6 Ga, and nine date between 2212 ±28 Ma and 1766 ±30 Ma (16%). 16 zircons are bracketed between 1044 ±33 Ma and 922 ±34 Ma (28%), and 22 date between 851 ±34 Ma and 544 ±37 Ma (41%) representing the most abundant age-population (Fig. 5E). One young zircon dates at 426 ±8 Ma ($^{206}Pb/^{238}U$ date concordant at 106%), and two younger $^{206}Pb/^{238}U$ date at 200 ±10 Ma and 190 ±10 Ma, concordant at 79% and 95%, respectively (Table 8).

Sample WP103 (the Kalahari Group)

Sample WP103 is taken from locally mined (diamondiferous) gravels of the Kalahari Group at Kitsaku Digging in the Kwango area (Fig. 3B). In this sample, zircons are coarse to very coarse (300-600 µm), both angular and well rounded, and of various color (Fig. 4E). In total 50 single zircon dates are concordant (Table 9). 31 date between 2958 ±26 Ma and 2491 ±27 Ma (62%), which represent the most abundant age-population (Fig. 5F). Three zircons date between 2294 ±29 Ma and 2158 ±28 Ma, five date at 1.9 Ga, one dates at 1.0 Ga (1058 ±20 Ma), and nine are between 734 ±34 Ma and 529 ±36 Ma (18%). Two young zircons have $^{206}Pb/^{238}U$ dates of 300 ±10 Ma ($^{206}Pb/^{238}U$ dates concordant at 79% and 91%), and the two youngest, which are large zircon fragments with very low U and Pb concentrations, date at 130-140 Ma (concordant at 12% and 34%). The latter could represent fragments of kimberlitic megacrysts but more analysis is needed to support this interpretation.

5. Discussion

In the different stratigraphic groups of the CB (the Inkisi, Lukuga, Haute Lueki, Kwango and Kalahari Groups) four main detrital zircon age-populations are found (Fig. 6A): 1) Archean to early Paleoproterozoic; 2) mid-Paleoproterozoic (Eburnian); 3) mid-Mesoproterozoic to early Neoproterozoic (Kibaran); and 4) late Neoproterozoic to early Cambrian (Pan African), although there are differences in their proportions. The occurrence of a small number (6) of Carboniferous-Jurassic zircons within the uppermost Kwango and Kalahari Groups suggests the emergence of younger source terrains during the late Mesozoic. This change coincides with the conspicuous (break-up) unconformity at the base of the Jurassic-Cretaceous succession in the CB (Fig. 2).

[Figure 6 here]

Archean to early Paleoproterozoic (3.1 Ga and 2.9-2.4 Ga)

Archean to early Paleoproterozoic dates are present in all the samples, albeit not the most abundant (13% in total; Fig. 6A). The oldest zircon dates at 3.1 Ga (3133 ±29 Ma), and the others range between 2959 ±26 Ma and 2428 ±16 Ma. These dates are the most abundant in the samples from the Kwango field study area and from the Dekese section (only one grain is from the Samba section). They may have been derived from a number of cratonic sources surrounding the CB (Fig. 6B; see de Wit and Linol, 2014, for review), for example: the ca. 2.9-2.7 Ga Kasai-Lomami and Dibaya Complexes of the Kasai and Cuango Cratons (Cahen et al, 1984; Delhal, 1991); the 3.2-2.7 Ga Ntem Complex and Nyong Series (Caen-Vachette et al., 1988; Feybesse et al., 1998; Nkoumbou et al., 2013), the 3.0-2.6 Ga Mboumou-Uganda Craton (Link et al., 2010; Mänttäri et al., 2013), the Tanzanian Craton (e.g. the 3.1-2.5 Ga Dodoman Complex; Kabete et al. 2012; Lawley et al., 2013). Other possible sources are from surrounding Proterozoic belts, such as for example from the Mbuji-Mayi and Muva sequences in southeastern DRC, which contain Archean detrital zircons (Rainaud et al., 2003; Delpomdor et al., 2013). In the sample from the (Kalahari) Kwango river terraces, however, the predominant dates of 2715 Ma most likely correspond to migmatites and pegmatites of the Dibaya Complex (the Cuango Craton), outcropping immediately upstream along a major knickpoint, as indicated by the large size and angular shape of the zircons (Fig. 5F).

Mid-Paleoproterozoic (2.2-1.8 Ga)

Mid-Paleoproterozoic dates are represented in all the samples (18% in total; Fig. 6A), but are much more abundant in the samples from the Lukuga diamictites in the Dekese section (Fig. 5B). These dates, mainly ranging between 2.0 Ga and 1.8 Ga, correspond to widely outcropping Eburnian rock sequences in east Africa (e.g. the Toro and Ubendian Belts; Link et al., 2010; Boniface et al., 2012), as indicated by the westward direction of paleocurrents for the Lukuga Group (Fig. 6B).

Mesoproterozoic to early Neoproterozoic to (1600-850 Ma)

Mesoproterozoic to early Neoproterozoic dates are abundant in all the samples (33% in total; Fig. 6A), indicating important and prolonged contributions from Kibaran aged-terrains to the sediment sources for the CB. In the samples from the Lukuga Group five zircons dated between 1421 ±16 Ma and 1371 ±18 Ma. This coincides with the Kibaran-age Belt (sensu stricto) along the eastern margin of the basin (Fig. 6B), dated at ca. 1375 Ma (Tack et al., 2010). The lack of detrital zircons of this age (1.4 Ga) in all the other samples suggests that this large region of east-central Africa was not a major source for the CB, possibly because it was covered by later sediments or because it remained below sea level.

In all samples from all the stratigraphic sequences, most of other dates are bracketed between 1100 Ma and 950 Ma (Fig. 6A). In addition, repeated analysis on some zircons of this age also gave younger dates of 750 Ma, 700 Ma and 650 Ma, providing evidence for local recrystallization during the late Neoproterozoic. This suggests partial reworking during the Pan African orogens. Such dates are most common within the Oubanguides, in particular the ca. 1000-600 Ma Central Saharan Belt in CAR and North African Shield (e.g. in Chad; de Wit et al., 2005, and 2014; Toteu et al., in preparation), and on the South American flank of the Atlantic Ocean, especially within the Sergipano-Araguaia Belts in northeastern Brazil (e.g. dos Santos et al., 2010; de Brito Neves, 2011). These (distant) northern provenances for the CB are supported by other recent detrital zircon studies that found also dominant 1.0 Ga age-populations within the upper Neoproterozoic to lower Paleozoic West Congo and Inkisi Groups along the western margin of the basin (Frimmel et al., 2006; Jelsma et al., 2011). Such Pan African metasediments and associated molasses-like basin sequences, abundantly exposed around the margins of the CB, and which were regionally derived from the north (Alvarez et al., 1995; Master et al., 2005; Figs. 6B and 7), may also have constituted significant secondary sources for the sediments.

Late Neoproterozoic to Cambrian (850-500 Ma)

Late Neoproterozoic to Cambrian zircon dates are also abundant in all the samples (35% in total; Fig. 6A). This series of dates, relatively continuous between 800 Ma and 540 Ma, corresponds to several episodes of the Pan African orogens. However, possible sources with this age-range are abundant within the Pan African mobile belts that surround the CB, and at this stage it is not possible to differentiate between these widely dispersed terrains. Sediment dispersal directions (Fig. 6B) favor Pan African provinces located to the north (the Oubanguides), and to the east and southeast (the Mozambique and Lufilian Belts). In addition, the general increase in abundance of this 850-500 Ma zircon age-population from the Paleozoic (Inkisi and Lukuga) to the Mesozoic sequences (Haute Lueki and Kwango) could suggest sustained Phanerozoic exhumation of the surrounding Pan African mobile belts, and/or progressive concentration by recycling Paleozoic sediments (Fig. 7).

[Figure 7 here]

Late Carboniferous-Jurassic (300-240 and 190 Ma)

Six young zircons, small in size and displaying no magmatic zoning, dated at 300-240 Ma and 190 Ma in the Kwango and Kalahari Groups indicate some contributions from Upper Carboniferous-Lower Jurassic sources to the CB. These dates may possibly correspond to Permian-Triassic kimberlites and Karoo flood basalts in northern Angola (Jelsma personal communication in 2011). However, it is more likely that these fine and delicate zircons are related to ash fallouts linked to extensive late Paleozoic-Jurassic felsic volcanism and magmatism of the Choiyoi and Chon Aike Provinces in western Argentina and Chile (Mpodozis and Kay, 1992; Ramos and Aleman, 2000; Munizaga et al., 2008). For instance, such air-fall tuffs are commonly recorded in the Permian-Triassic sedimentary rocks of the Paraná and Karoo Basins of southwestern Gondwana (Bangert et al., 1999; Guerra-Sommer et al., 2008; Milani and de Wit, 2008; Fildani et al., 2009; Rocha-Campos et al., 2011). In the southern CB, however, paleo-wind directions measured from the Kwango aeolianites (e.g. Fig. 3A) indicate strong near surface winds to the southwest. Thus, this suggests (opposite) north-directed upper atmospheric circulations across interior Gondwana, episodically transporting volcanic dust originated from volcanoes above the Andean subduction margin of Gondwana, more than 5000 km northward to the CB (Fig. 8).

[Figure 8 here]

Conclusions

U-Pb dates from 568 detrital zircons of the Phanerozoic successions in the CB characterize the evolution of source provenances during the development of this largest basin of central Gondwana. The four main age-populations documented in this study (ca. Archean, Eburnian, Kibaran and Pan African) can be linked to potential sources within the Precambrian basement immediately surrounding the CB. An exception is a prominent peak at 950-1100 Ma (Fig. 6A), for which the most likely (larger) sources are within the Oubanguides and the North African Shield (e.g. Darfour), and the Brasiliano Belts in northeastern Brazil, since their upper Neoproterozoic sequences and associated sedimentary cover are widespread around the CB and given that these sequences regionally derived from the north. In contrast, input from the ca. 1.4 Ga Kibaran Belt is limited to the east-derived, Carboniferous glacial deposits of the CB. This suggests that east-central Africa was mostly not a major source for the sediments, possibly because this region was covered by sediments or remained below sea-level throughout the late Paleozoic-Mesozoic, as supported by sedimentological and biostratigraphic data. In addition, some younger zircons dated at 290 Ma, 240 Ma, 200 Ma and 190 Ma in the Jurassic-Cretaceous aeolian red sandstones reflects the influence of new Permian-Jurassic sources during the Mesozoic. We interpret those to be derived from air-fall tuffs related to far-field volcanic activity of the proto-Andes flanking the southwest margin of Gondwana (Figs. 7 and 8).

Acknowledgments

We acknowledge funding through the Inkaba yeAfrica and !Khure Africa programs, supported by the DST/NRF of South Africa. We thank Max Fernandez-Alonso, Damien Delvaux and Edmond Thorose for accessing the archived cores at the Royal Museum for Central Africa (RMCA), and Ulrich Glasmacher for providing some of the zircon concentrates from the lower parts of the boreholes. B. Linol particularly thanks Hielke Jelsma for discussions about the CB. We also thank S. Master and an anonymous reviewer for their comments. This is AEON contribution number 136 and Inkaba yeAfrica contribution number 115.

References

Alvarez, P., Maurin, J.C., and Vicat, J.-P., 1995. La Formation de l'Inkisi (Supergroupe Ouest-congolien) en Afrique centrale (Congo et Bas-Zaire): un delta d'âge Paléozoique comblant un bassin en extension. Journal of African Earth Sciences, 20(2), p.119-131.

Antunes, M.T., Maisey, J.G., Marques, M.M., Schaeffer, B., and Thomson, K.S., 1990. Triassic fishes from the Cassange Depression (R.P. de Angola). Universitade de Lisboa, Ciencias da Terra, Numero Esp, p.1-64.

Bangert, B., Stollhofen, H., Lorenz, V., and Armstrong, R., 1999. The geochronology and significance of ash-fall tuffs in the glaciogenic Carboniferous-Permian Dwyka Group of Namibia and South Africa. Journal of African Earth Sciences, 29(1), p.33-49.

Belshaw, N.S., Freedman, P.A., O'Nions, R.K., Frank, M., and Guo, Y., 1998. A new variable dispersion double-focussing plasma mass spectrometer with performance illustrated for Pb isotopes. International Journal of Mass Spectrometry, 181, p.51-58.

Biggin, A.J., de Wit, M.J., Langereis, C.G., Zegers, T.E., Voûte, S., Dekkers, M.J., and Drost, K., 2011. Palaeomagnetism of Archean rocks of the Onverwacht Group, Barberton Greenstone Belt (southern Africa): Evidence for a stable and potentially reversing geomagnetic field at ca. 3.5 Ga. Earth and Planetary Science Letters, 302(3-4), p.314-328.

Bingen, B., Jacobs, J., Viola, G., Henderson, I.H.C., Skår, Ø., Boyd, R., Thomas, R.J., Solli, A., Key, R.M., and Daudi, E.X.F., 2009. Geochronology of the Precambrian crust in the Mozambique belt in NE Mozambique, and implications for Gondwana assembly. Precambrian Research, 170(3-4), p.231-255.

Boniface, N., Schenk, V., Appel, P. 2012. Paleoproterozoic eclogites of MORB-type chemistry and three Proterozoic orogenic cycles in the Ubendian Belt (Tanzania): Evidence from monazite and zircon geochronology, and geochemistry. Precambrian Research 192-195, p.16– 33.

Bordy, E.M., Segwabe, T., and Makuke, B., 2010. Sedimentology of the Upper Triassic-Lower Jurassic (?) Mosolotsane Formation (Karoo Supergroup), Kalahari Karoo Basin, Botswana. Journal of African Earth Sciences, 58(1), p.127-140.

Bose, M.N., and Kar, R.K., 1976. Palaeozoic *sporae dispersae* from Zaïre (Congo). XI: Assises glaciaires et periglaciaire from the Lukuga Valley. Annales du Musée Royal de l'Afrique centrale, Tervuren (Belgique), Série in 8, Sciences Geologiques, 77, p.1-19.

Bose, M.N., and Kar, R.K., 1978. Biostratigraphy of the Lukuga Group in Zaire. Annales du Musée Royal de l'Afrique centrale, Tervuren (Belgique), Série in 8, Sciences Geologiques, 82, p.97-114.

Boulouard, C., and Calandra, F., 1963. Etude palynologique de quelques sondages de la République du Congo (Congo ex-Belge). Unpublished report R/ST-no.7376, SNPA Direction exploration et production Pau, France.

Boutakoff, N., 1948. Les formations glaciaires et post-glaciaires fossilifères, d'âge permo-carbonifère (Karoo inférieur) de la region de Walikale (Kivu, Congo belge). Mémoire de l'Institut géologique. Université de Louvain, IX (II), 214 pp.

Buiter, S.J.H., Steinberger, B., Medvedev, S., and Tetreault, J.L., 2012. Could the mantle have caused subsidence of the Congo Basin? Tectonophysics, 514-517, p.62-80.

Caen-Vachette, M., Vialette, Y., Bassot, J.-P., and Vidal, P., 1988. Apport de la géochronologie isotopique à la connaissance de la géologie gabonaise. Chroniques de la recherche minière, 491, p.35-54.

Cahen, L., 1954. Géologie du Congo Belge. Liège: Vaillant-Carmanne, 577pp.

Cahen, L., 1981. Précisions sur la stratigraphie et les corrélations du Goupe de la Haute-Lueki et des formations comparables (Triasique a Liasique? d'Afrique Centrale). Rapport annuel du Musée Royal d'Afrique centrale, Tervuren (Belgique), Départment de Géologie et de Minéralogie, p.81-96.

Cahen, L., 1983a. Le Groupe de Stanleyville (Jurassic superieur et Wealdien de l'intérieur de la République du Zaïre): Révision des connaissances. Rapport annuel du Musée Royal de l'Afrique centrale, Tervuren (Belgique), Département de Géologie et de Minéralogie, p.73-91.

Cahen, L., 1983b. Brèves précisions sur l'âge des groupes crétaciques post-Wealdien (Loia, Bokungu, Kwango) du Bassin interieur du Congo (Republique du Zaïre). Rapport annuel du Musée Royal de l'Afrique centrale, Tervuren (Belgique), Département de Géologie et de Minéralogie, p.61-72.

Cahen, L., and Lepersonne, J., 1978. Synthèse des connaissances relatives au Groupe (anciennement Série) de la Lukuga (Permien du Zaïre). Annales du Musée

Royal du Congo belge, Tervuren (Belgique), Série in-8, Sciences géologiques, 82, p.115-152.

Cahen, L., Ferrand, J.J., Haarsma, M.J.F., Lepersonne, J., and Verbeek, T., 1959. Description du Sondage de Samba. Annales du Musée Royal du Congo belge, Tervuren (Belgique), Série in-8, Sciences géologiques, 29, 210p.

Cahen, L., Ferrand, J.J., Haarsma, M.J.F., Lepersonne, J., and Verbeek, T., 1960. Description du Sondage de Dekese. Annales du Musée Royal du Congo belge, Tervuren (Belgique), Série in-8, Sciences géologiques, 34, 115p.

Cahen, L., Snelling, N.J., Delhal, J., and Vail, J., 1984. The Geochronology and Evolution of Africa. Oxford: Clarendon Press, 512pp.

Casier, E., 1965, Poissons fossiles de la Série du Kwango (Congo). Annales du Musée royal de l'Afrique Centrale, Tervuren (Belgique), Série in-8, Sciences géologiques, 50, 69p.

Catuneanu, O., Wopfner, H., Eriksson, P.G., Cairncross, B., Rubidge, B.S., Smith, R.M.H., and Hancox, P.J., 2005. The Karoo basins of south-central Africa. Journal of African Earth Sciences, 43(1-3), p.211-253.

Cocherie, A., and Robert, M., 2008. Laser ablation coupled with ICP-MS applied to U-Pb zircon geochronology: A review of recent advances. Gondwana Research, 14, p.597-608.

Colin, J.-P., 1981. Paleontological study of the Esso/Texaco well Gilson-1, Zaire. Unpublished report EPR-E.WA19.81.

Colin, J.-P., 1994. Mesozoic-Cenozoic lacustrine sediments in the Zaïre Interior Basin. In: Gierlowski-Kordesch, E., and Kelts, K. (eds.), Global Geological Record of Lake Basins. Cambridge University Press, 4, pp.31-36.

Colin, J.-P., and Jan du Chêne, J., 1981. Paleontological study of the Esso/Texaco well Mbandaka-1, Zaire. Unpublished report EPR-E.WA15.81.

Cox, L.R., 1960. Further mollusca from the Lualaba beds of the Belgian Congo. Annales du Musée Royal du Congo belge, Tervuren (Belgique), 37, p.1-15.

Crosby, A. G., Fishwick, S., and White, N., 2010. Structure and evolution of the intracratonic Congo Basin. Geochemistry Geophysics Geosystems, 11(6), p.1-20.

Daly, M.C., Lawrence, S.R., Kimun'a, D., and Binga, M., 1991. Late Paleozoic deformation in central Africa: a result of distant collision. Nature, 350, p.605-607.

Daly, M.C., Lawrence, S.R., Diemu-Tshiband, K., and Matouana, B., 1992. Tectonic evolution of the Cuvette Centrale, Zaire. Journal of the Geological Society, 149(4), p.539-546.

De Brito Neves, B.B., 2011. The Paleoproterozoic in the South-American continent: Diversity in the geologic time. Journal of South American Earth Sciences, 32, p.270-286.

De Carvalho, H., Tassinari, C., Alves, P.M., Guimarães, F., and Simões, M.C., 2000. Geochronological review of the Precambrian in western Angola: links with Brazil. Journal of African Earth Sciences, 31(2), p.383-402.

Defretin-Lefranc, S., 1967. Étude sur les phyllopodes du Bassin du Congo. Annales du Musée Royal de l'Afrique centrale, Tervuren (Belgique), Série in-8, Sciences géologiques, 56, 122p.

Delhal, J., 1991, Situation géochronologique 1990 du Precambrian du Sud-Kasai et de l'Ouest-Shaba. Rapport annuel du Musee Royal de l'Afrique centrale, Tervuren (Belgique), Département de Géologie et de Minéralogie, p.119-125.

Delpomdor, F., Linnemann, U., Boven, A., Gärtner, A., Travin, A., Blanpied, C., Virgone, A., Jelsma, H., and Préat, A., 2013. Depositional age, provenance, and tectonic and paleoclimatic settings of the late Mesoproterozoic-middle Neoproterozoic Mbuji-Mayi Supergroup, Democratic Republic of Congo. Palaeogeography, Palaeoclimatology, Palaeoecology, 389, p.4-34.

De Ploey, J., 1968. Sédimentologie et origine des sables de la série des sables ocre et de la série des 'grès polymorphes' (Système du Kalahari) au Congo Occidental. Annales du Musée Royal de l'Afrique centrale, Tavuren (Belgique), Série in-8, Sciences géologiques, 61, 72p.

De Waele, B., Johnson, S.P., and Pisarevsky, S.A., 2008. Palaeoproterozoic to Neoproterozoic growth and evolution of the eastern Congo Craton: Its role in the Rodinia puzzle. Precambrian Research, 160, p.127-141.

De Waele, B., Liégeois, J.-P., Nemchin, A.A., and Tembo, F., 2006. Isotopic and geochemical evidence of Proterozoic episodic crustal reworking within the Irumide belt of south-central Africa, the southern metacratonic boundary of an Archaean Bangweulu Craton. Precambrian Research, 148(3-4), p.225-256.

De Wit, M.J., 2009. Tsodilo Resources Limited drills extension of Zambian copper belt-like mineralization in Pan African Basement of northwest Botswana. Tsodilo Resources Ltd. Report. www.tsodiloresources.com

De Wit, M.J., Jeffery, M., Berg, H, and Nicolayson, L.O., 1988. Geological Map of sectors of Gondwana re-constructed to their position ~150 Ma (with explanatory notes), scale 1: 1.000.000. Tulsa: American Association of Petroleum Geologists.

De Wit, MJ, Bowring, S., Dudas, F., Kamga, G. 2005. The great Neoproterozoic central Saharan arc and the amalgamation of the north African Shield. GAC-MAC-CSPG-CSSS Conference, Halifax, Canada. Abstracts with programs, p43.

De Wit, M.J., de Brito Neves, B.B., Trouw, R.A.J., and Pankhurst, R.J., 2008. Pre-Cenozoic correlations across the South Atlantic region: “the ties that bind”. In: Pankurst, R.J., Trouw, R.A.J., Brito Neves, B.B., and de Wit, M.J. (eds.), West Gondwana: Pre-Cenozoic Correlations Across the South Atlantic Region. Geological Society of London, Special Publications, 294, pp.1-8.

De Wit, M.J., and Linol, B., 2014. Chapter 2: Precambrian basement of the Congo Basin and its flanking terrains. In: de Wit, M.J., Guillocheau, F., and de Wit, M.J.C. (Eds.), The Geology and Resource Potential of the Congo Basin, Springer-Verlag, in press.

De Wit, M.J., Bowring, S., Buchwaldt, R., Dudas, F., MacPhee, D, Tagne-Kamga, G., Dunn, N., Salet, A.M., and Nambatingar, D. 2014. Proterozoic crust of the Central Sahara Shield. (Submitted to Gondwana Research).

Dos Santos, E.J., von Schmus, W.R.V., Kozuch, M., and Neves, B.B.D.B., 2010. The Cariris Velhos tectonic event in Northeast Brazil. Journal of South American Earth Sciences, 29(1), p.61-76.

Esso-Zaire SARL, 1981a. Geological Completion Report: Gilson-1. Unpublished report.

Esso-Zaire SARL, 1981b. Geological Completion Report: Mbandaka-1. Unpublished report.

Evrard, P., 1960. Sismique. Annales du Musée Royal du Congo belge, Tervuren (Belgique), Série in-8, Sci-ences géologiques, 33, 87p.

Fedo, C.M., Sircombe, K.N., and Rainbird, R.H., 2003. Detrital zircon analysis of the sedimentary record. Reviews in Mineralogy and Geochemistry, 53(1), p.277-303.

Fernandez-Alonso, A., Cutten, H., De Waele B., Tack, L., Tahon, A., Baudet, D., and Barritt, S.D., 2012. The Mesoproterozoic Karagwe-Ankole Belt (formerly the NE Kibara Belt): The result of prolonged extensional intracratonic basin development punctuated by two short-lived far-field compressional events. Precambrian Research, 216-219, p.63-86.

Feybesse, J.L., Johan, V., Triboulet, C., Guerrot, C. Mayaga-Mikolo, F., Bouchot, V., Eko N'Dong, J., 1998. The West Central African belt: a model of 2.5-2.0 Ga accretion and two-phase orogenic evolution. Precambrian Research, 87, p.161-216.

Fildani, A., Weislogel, A., Drinkwater, N.J., McHargue, T., Tankard, A., Wooden, J., Hodgson, D., and Flint, S., 2009. U-Pb zircon ages from the southwestern Karoo Basin, South Africa: Implications for the Permian-Triassic boundary. Geology, 37(8), p.719-722.

Frimmel, H., Tack, L., Basei, M., Nutman, A, and Boven, A, 2006. Provenance and chemostratigraphy of the Neoproterozoic West Congolian Group in the Democratic Republic of Congo. Journal of African Earth Sciences, 46(3), p.221-239.

Fritz, H., Abdelsalam, M., Ali, K.A., Bingen, B., Collins, A.S., Fowler, A.R., Ghebreab, W., Hauzenberger, C.A., Johnson, P.R., Kusky, T.M., P. Macey, P., S. Muhongo, S., Stern, R.J., Viola, G. 2013. Orogen styles in the East African Orogen: A review of the Neoproterozoic to Cambrian tectonic evolution. Journal of African Earth Sciences, 86, 65–106.

Giresse, P., 2005. Mesozoic-Cenozoic history of the Congo Basin. Journal of African Earth Sciences, 43, p.301-315.

Grékoff, N., 1957. Ostracodes du Bassin du Congo. I. Jurassique supérieur et Crétace inférieur du nord du basin. Annales du Musée Royal de l'Afrique centrale, Tervuren (Belgique), Série in-8, Sciences géologiques, 19, 97p.

Grékoff, N., 1958. Ostracodes du Bassin du Congo. III. Tertiaire. Annales du Musée Royal de l'Afrique centrale, Tervuren (Belgique), Série in-8, Sciences géologiques, 22, 36p.

Grékoff, N., 1960. Ostracodes du Bassin du Congo. II. Crétacé. Annales du Musée Royal de l'Afrique centrale, Tervuren (Belgique), Série in-8, Sciences géologiques, 22, 36p.

Guerra-Sommer, M., Cazzulo-Klepzig, M., Laquintinie Formoso, M.L., Menegat, R., and Mendonça Fo, J.G., 2008. U-Pb dating of tonstein layers from a coal succession of the southern Paraná Basin (Brazil): A new geochronological approach. Gondwana Research, 14(3), p.474-482.

Jamal, D.L., 2005. Crustal studies across selected geotransects in NE Mozambique: Differentialting between Mozambican (-Kibaran) and Pan Africa events, with implications for Gondwana studies. Unpublished PhD Thesis, University of Cape Town, 365 pp.

Jamotte, A., 1932. Contribution à l'étude géologique du basin charbonnier de la Lukuga. Annales du Service des Mines, Tome II, Comité Spécial du Katanga, p.1-75.

Jelsma, H.A, Perrit, S.H., Amstrong, R., and Ferreira, H.F., 2011. Shrimp U-Pb zircon geochronology of basement rocks of the Angolan Shield, western Angola. Abstract, 23rd CAG, Johannesburg, 8th-14th January.

Johnson, M.R., van Vuuren, C.J., Hegenberger, W.F., Key, R., and Shoko, U., 1996. The Stratigraphy of the Karoo Supergroup in southern Africa: an overview. Journal of African Earth Sciences, 23(1), p.3-15.

Jokat, W., Boebel, T., König, M., and Meyer, U., 2003. Timing and geometry of early Gondwana breakup. Journal of Geophysical Research: Solid Earth, 108(B9).

Jones, L., Mathieu, P.L., and Strenger, H., 1959. Magnétisme. Annales du Musée Royal de l'Afrique central, Tervuren (Belgique), Série in-8, Sciences géologiques, 27, 30p.

Kadima, E., Delvaux, D., Sebagenzi, S.N., Tack, L., and Kabeya, S.M., 2011. Structure and geological history of the Congo Basin: an integrated interpretation of gravity, magnetic and reflection seismic data. Basin Research, 23(5), p.499-527.

Kamo, S.L., and Davis, D.W., 1994. Reassessment of Archean crustal development in the Barberton Mountain Land, South Africa, based on U-Pb dating. Tectonics, 13(1). P.167-192.

Kanda N.V., Mpiana, C., Cibambula, E., Fernandez-Alonso, M., Delvaux, D., Kadima, E., Delpomdor, F., Tahon, A., Dumont, P., Hanon, M., Baudet, D., de Waele, S., and Tack, L., 2011. The 1000 m thick Redbeds sequence of the Congo River Basin (CRB): a generally overlooked testimony in Central Africa of post-Gondwana amalgamation (550 Ma) and pre-Karoo break-up (320 Ma). Abstract, 23rd CAG, Johannesburg, 8th-14th January.

Lawley, C.J.M., Selby, D., Condon, D.J., Horstwood, M., Millar, I., Crowley, Q., Imber, J. 2013. Lithogeochemistry, geochronology and geodynamic setting of the Lupa Terrane, Tanzania: Implications for the extent of the Archean Tanzanian Craton. Precambrian Research, 231, p.174-193.

Lawrence, S.R., and Makazu, M.M., 1988. Zaire's Central Basin: Prospectivity outlook. Oil & Gas Journal, 86(38), p.105-108.

Lenoir, J.L., Liegeois, J.-P., Theunissen, K., and Klerkx, J., 1995. The Palaeoproterozoic Ubendian shear belt in Tanzania: geochronology and structure. Journal of African Earth Sciences, 19(3), p.169-184.

Lepersonne, J., 1951. Les subdivisions du système du Karoo au Kwango (Congo belge). Annales de la Société Géologique de Belgique, LXXIV, p.123-138.

Lepersonne, J., 1974. Carte géologique du Zaïre au 1: 2.000.000 + Notice explicative. Kinshasa, République du Zaïre: Direction de la Géologie/Musée Royal de l'Afrique centrale, Tervuren (Belgique).

Leriche, M., 1927. Les fossiles des grès polymorphes (couches de Lubilash) aux confins du Congo et de l'Angola. Annales de la Société Géologique de Belgique, 50, p.44-51.

Lerouge, C., Cocherie, A., Toteu, S.F., Penaye, J., Milési, J.-P., Tchameni, R., Nsifa, E.N., Fanning, C.M., and Deloule, E., 2006. Shrimp U-Pb zircon age evidence for Paleoproterozoic sedimentation and 2.05 Ga syntectonic plutonism in the Nyong Group, South-Western Cameroon: consequences for the Eburnean-Transamazonian belt of NE Brazil and Central Africa. Journal of African Earth Sciences, 44(4-5), p.413-427.

Link, K., Koehn, D., Barth, M.G., Aanyu, K., and Foley, S.F., 2010. Continuous cratonic crust between the Congo and Tanzania blocks in western Uganda. International Journal of Earth Sciences (Geologische Rundschau), 99, p.1559-1573.

Linol, B., 2013. Sedimentology and sequence stratigraphy of the Congo and Kalahari Basins of south-central Africa and their evolution during the formation and break-up of West Gondwana. PhD thesis, Nelson Mandela Metropolitan University, 375p.

Linol, B., de Wit, M.J., Barton, E., Guillocheau, F., de Wit, M.J.C, and Colin. J.-P., 2014a. Chapter 7: Paleogeography and tectono-stratigraphy of Carboniferous-Permian and Triassic 'Karoo-like' sequences of the Congo Basin. In: de Wit, M.J., Guillocheau, F., and de Wit, M.J.C. (Eds.), The Geology and Resource Potential of the Congo Basin, Springer-Verlag, in press.

Linol, B., de Wit, M.J., Barton, E., Guillocheau, F., de Wit, M.J.C, and Colin. J.-P., 2014b. Chapter 8: Facies analysis, chronostratigraphy, and paleo-environmental reconstructions of the Jurassic to Cretaceous sequences of the Congo Basin. In: de Wit, M.J., Guillocheau, F., and de Wit, M.J.C. (Eds.), The Geology and Resource Potential of the Congo Basin, Springer-Verlag, in press.

Linol, B., de Wit, M.J., Guillocheau, F., Robin, C. and Dauteuil, O., 2014c. Chapter 11: Multiphase Phanerozoic subsidence and uplift history recorded in the Congo Basin – a complex successor basin. In: de Wit, M.J., Guillocheau, F., and de

Wit, M.J.C. (Eds.), The Geology and Resource Potential of the Congo Basin, Springer-Verlag, in press.

Linol, B., de Wit, M.J., Milani, E.J., Guillocheau, F. and Scherer, C. 2014d. Chapter 13: New regional correlations between the Congo, Paraná and Cape-Karoo Basins of southwest Gondwana. In: de Wit, M.J., Guillocheau, F., and de Wit, M.J.C. (Eds.), The Geology and Resource Potential of the Congo Basin, Springer-Verlag, in press.

Lombard, A.L., 1961. La série de la Haute Lueki (partie orientale de la cuvette congolaise). Bulletin de la Société belge de Géologie, de Paléontologie et d'Hydrologie, 70, p.65-72.

Ludwig, K.R., 2003. Isoplot/version 3.0: A geochronological toolkit for Microsoft Excel. Berkeley Geochro-nology Center Special Publication, 4, 71p.

Maheshwari, H., Bose, M.N., and Kumaran, K.P., 1977. Mesozoic *sporae dispersae* from Zaire. II: The Loia and Bokungu Groups in the Samba borehole. III: Some miospores from the Stanleyville Group. Annales du Musée Royal de l'Afrique centrale, Tervuren (Belgique), Série in-8, Sciences géologiques, 80, 60p.

Marlière, R., 1950. Ostracodes et phyllopodes du système du Karoo au Congo Belge. Annales du Musée du Congo belge, 6, p.1-43.

Master, S., Rainaud, C., Armstrong, R., Phillips, D., and Robb, L., 2005. Provenance ages of the Neoproterozoic Katanga Supergroup (Central African Copperbelt), with implications for basin evolution. Journal of African Earth Sciences, 42(1-5), p.41-60.

Milani, E.J., and de Wit, M.J., 2008. Correlations between the classic Paraná and Cape Karoo sequences of South America and southern Africa and their basin infills flanking the Gondwanides: du Toit revisited. In: Pankurst, R.J., Trouw, R.A.J., Brito Neves, B.B., and de Wit, M.J. (eds.), West Gondwana: Pre-Cenozoic Correlations Across the South Atlantic Region. Geological Society of London, Special Publications, 294, pp.319-342.

Milani, E.J., Gonçalves de Melo, J.H., de Souza, P.A., Fernandes, L.A., and França, A.B., 2007. Bacia do Pa-raná. Boletim de geociências da petrobras, 15 (2), pp.265-287.

Miller, R., 2008. The Geology of Namibia, Volume 3: upper Palaeozoic-Cenozoic. Windhoek, Namibia: Geological Survey.

Munizaga, F., Maksaev, V., Fanning, C.M., Giglio, S., Yaxley, G., and Tassinari, C.C.G., 2008. Late Paleozoic-Early Triassic magmatism on the western margin of Gondwana: Collahuasi area, Northern Chile. Gondwana Research, 13(3), p.407-427.

Nkoumbou, C., Barbey, P., Yonta-Ngouné, C., Paquette, J.L., and Villiéras, F., 2013. Pre-collisional geodynamic context of the southern margin of the Pan-African fold belt in Cameroon. Journal of African Earth Sciences, http://dx.doi.org/10.1016/j.jafrearsci.2013.10.002.

Pedrosa-Soares, A.C., Alkmim, F.F., Tack, L., Noce, C.M., Babinski, M., Silva, L.C., and Martins-Neto, M.A., 2008, Similarities and differences between the Brazilian and African counterparts of the Neoproterozoic Araçuaí-West Congo orogen. Geological Society, London, Special Publications, 294(1), p.153-172.

Poidevin, J.L., 1985. Le Proterozoique supérieur de la Républic Centrafricaine. Annales du Musée Royal de l'Afrique centrale, Tervuren (Belgique), Serie in-8, Sciences Geologiques, 91, 75p.

Polinard, E., 1932. Découverte des gisements fossilifères d'eau douce sur les versants de la Lubudi au Katanga méridional. Annales de la Société Géologique de Belgique, 55, p.63-81.

Rainaud, C., Master, S., Armstrong, R.A. and Robb, L.J., 2003. A cryptic Mesoarchaean terrane in the basement to the Central African Copperbelt. Journal of the Geological Society of London, 160, p.11-14.

Ramos, V.A., and Aleman, A., 2000. Tectonic Evolution of the Andes. In: Cordani, U.G., Milani, E.J., Thomaz Filho, A., and Campos, D.A. (eds.), Tectonic Evolution of South America. Rio de Janeiro, Brazil: 31st international geological congress, p.635-685.

Rankin, W., Webb, S.J., Kiyan, D., Kinnaird, J.A., Jones, A.G. and Evans, R.L. (2013). Linking the Damara (Namibia) and Lufilian/Katangan (Zambia) belts through geophysical interpretations. Proceedings of the 13th SAGA Biennial Conference and Exhibition, Kruger Park, South African Geophysical Association, 4 pp.

Reeves, C.V., 1999. Aeromagnetic and gravity features of Gondwana and their relation to continental break-up: more pieces, less puzzle. Journal of African Earth Sciences, 28, p.263-277.

Robert, M., 1946. Le Congo physique. Troisième edition. Liége: H. Vaillant-Carmanne, 449pp.

Rocha-Campos, A.C., Basei, M.A., Nutman, A.P., Kleiman, L.E., Varela, R., Llambias, E., Canile, F.M., and da Rosa, O.D.C.R., 2011. 30 million years of Permian volcanism recorded in the Choiyoi igneous province (W Argentina) and the source for younger ash fall deposits in the Paraná Basin: SHRIMP U-Pb zircon geochro-nology evidence. Gondwana Research, 19(2), p.509-523.

Rolin, P., 1995. Carte tectonique de la Republique centrafricaine, au 1:1.500.000. BRGM.

Sachse, V.F., Delvaux, D. and Littke, R., 2012. Petrological and geochemical investigations of potential source rocks of the central Congo Basin, DRC. American Association of Petroleum Geologists Bulletin, 96(2), p.245-275.

Saint Seine, P., 1953. Poissons de la cuvette congolaise. Compte rendus de la Société géologique de France, 16, p.343-345.

Saint Seine, P., 1955. Poissons fossiles de l’étage de Stanleyville (Congo belge). 1ère partie: La faune des argilites et schistes bitumineux. Annales du Musée Royal de l’Afrique centrale, Tervuren (Belgique), Série in 8, Sciences Géologiques, 14, 126p.

Saint Seine, P., and Casier, E., 1962. Poissons fossiles des couches de Stanleyville (Congo). 2ème partie: La faune marine des calcaires de Songa. Annales du Musée Royal de l’Afrique centrale, Tervuren (Belgique), Série in 8, Sciences Géologiques, 44, 52p.

Simonetti, A., Heaman, L.M., Hartlaub, R.P., Creaser, R.A., MacHattie, T.G., Böhm, C., 2005. U–Pb zircon dating by laser ablation-MC-ICP-MS using a new multiple ion counting Faraday collector array. Journal of Analytical Atomic Spectrometry, 20, p.677-686.

Sláma, J., Košler, J., Condon, D.J., Crowley, J.L., Gerdes, A., Hanchar, J.M., Horstwood, M.S.A., Morris, G.A., Nasdala, L., Norberg, N., Schaltegger, U., Schoene, B., Tubrett, M.N., and Whitehouse, MJ., 2008. Plešovice zircon – A new natural reference material for U-Pb and Hf isotopic microanalysis. Chemical Geology, 249, p.1-35.

Sommer, H., Kröner, A., Hauzenberger, C., Muhongo, S., and Wingate, M.T.D., 2003. Metamorphic petrology and zircon geochronology of high-grade rocks from the central Mozambique Belt of Tanzania: crustal recycling of Archean and Palaeoproterozoic material during the Pan-African orogeny. Journal of Metamorphic Geology, 21, p.915-934.

Tack, L., Wingate, M.T.D., and Lie, J., 2001. Early Neoproterozoic magmatism (1000-910 Ma) of the Zadinian and Mayumbian Groups (Bas-Congo): onset of Rodinia rifting at the western edge of the Congo craton. Precambrian Research, 110, p.277-306.

Tack, L., Wingate, M.T.D., de Waele, B., Meert, J., Belousova, E., Griffin, B., Tahon, A., and Fernandez-Alonso, M., 2010. The 1375 Ma "Kibaran event" in Central Africa: Prominent emplacement of bimodal magmatism under extensional regime. Precambrian Research, 180(1-2), p.63-84.

Tankard, A., Welsink, H., Aukes, P., Newton, R. and Stattker, E., 2012. Chapter 23: Geodynamic interpretation of the Cape and Karoo basins, South Africa. In: Roberts, D.G. and Bally, A.W. (Eds.). Phanerozoic Passive Margins, Cratonic Basins and Global Tectonics Maps. Amsterdam: Elsevier. pp.869-945.

Tait, J., Delpomdor, F., Preat, A., Tack, L., Straathof, G., and Nkula, V.K., 2011. Neoproterozoic sequences of the West Congo and Lindi/Ubangi Supergroups in the Congo Craton, Central Africa. In: Arnaud, E., Halverson, G.P., and Shields-Zhou, G. (eds.), The Geological Record of Neoproterozoic Glaciations. Geological Society of London, Memoirs, 36, pp.185-194.

Toteu, S.F., Van Schmus, W.R., Penaye, J., and Michard, A., 2001. New U-Pb and Sm-Nd data from north-central Cameroon and its bearing on the pre-Pan African history of central Africa. Precambrian Research, 108(1-2), p.45-73.

Toteu, S.F., Fouateu, R.Y., Penaye, J., Tchakounte, J., Mouangue, A.C.S., van Schmus, W.R., Deloule, E., and Stendal, H., 2006. U-Pb dating of plutonic rocks involved in the nappe tectonic in southern Cameroon: consequence for the Pan-African orogenic evolution of the central African fold belt. Journal of African Earth Sciences, 44(4-5), p.479-493.

Taverne, L., 1975, Etude ostéologique de *Leptolepis caheni*, Téléostéen fossile du Jurassique supérieur (Kimmeridgien) de Kisangani (ex-Stanleyville, Zaïre) précédemment décrit dans le genre *Paraclupavus*. Revue Zoologique Africaine, 89, p.821-853.

Taverne, L., 1976, Les téléostéens fossiles du crétacé moyen de Kipala (Kwango, Zaïre). Annales du Musée Royal de l'Afrique centrale, Tervuren (Belgique), Série in-8, Sciences géologiques, 79, 50p.

Torsvik, T.H., van der Voo, R., Preeden, U., Mac Niocaill, C., Steinberger, B., Doubrovine, P.V., van Hinsbergen, D.J.J., Domeier, M., Gaina, C., Tohver, E., Meert, J.G., McCausland, P.J.A., and Cocks, L.R., 2012. Phanerozoic Polar Wander, Palaeogeography and Dynamics. Earth Science Reviews, 114 (3-4), p.325-368.

Trouw, R.A., and de Wit, M.J., 1999. Relation between the Gondwanide Orogen and contemporaneous intracratonic deformation. Journal of African Earth Sciences, 28(1), p.203-213.

Zerfass, H., Chemale, F., Schultz, C.L., and Lavina, E., 2004. Tectonics and sedimentation in southern South America during the Triassic. Sedimentary Geology, 166(3-4), p.265-292.

Figures

Figure 1: (A) Tectonic map of the Precambrian basement of central Gondwana (inset for location) showing the Central African Shield (dotted line), and (B) main Phanerozoic sequences of central Africa, with location of the field study area and the four deep boreholes in the CB (updated from de Wit et al., 1988, 2008, and de Wit and Linol, 2014). Red outline marks the watershed of the modern CB drainage system.

Figure 2: Borehole litho- and bio-stratigraphic correlations across the central CB (Fig. 1B for location), showing the location of core-samples with dated detrital zircons (simplified from Linol, 2013, and Linol et al., 2014a). U1, U2 and U3 mark major unconformities determined from analysis of seismic.

Figure 3: Photos of outcrops along the Kwango River, southwest DRC (Fig. 1B for location), showing the location of samples. (A) Cliff of red sandstones near Swamasangu; cross-bed sets up to 10 m thick are characteristic of Jurassic-Cretaceous aeolian dune deposits. Paleocurrent measurements (n: 49) indicate predominant paleo-winds blowing to the southwest and to the south (Linol, 2013; see also Linol et al., 2014b). (B) Locally mined gravels at Kitsaku infill an irregular erosion surface (dotted line) incised into Karoo (late Paleozoic) conglomerates and red siltstones.

Figure 4: Microphotographs of selected zircons collected from the Kwango field study area (WP103; Fig. 3B), and from the Samba (S) and Dekese (D) cores; sample numbers refer to depth below surface (see Fig. 2).

Figure 5: Examples of backscatter electron microprobe images (left), Concordia diagrams (middle) and frequency plots (right) of U-Pb dated detrital zircons from main Phanerozoic groups of the CB (Figs. 2 and 3 for samples location). Numbers of zircon with a distinct age-range are plotted at the top of the frequency plots.

Figure 6: (A) Frequency plot of all U-Pb single zircon dates from the CB, and (B) simplified map of Precambrian basement ages (modified from Linol, 2013 and de Wit and Linol, 2014), with main sediment dispersal directions.

Figure 7: Paleo-reconstructions (left; modified from Scotese, 2014) and schematic diagrams (right) showing the paleogeography and paleo-topographic evolution of the CB in central Gondwana. (A) Upper Neoproterozoic-lower Paleozoic Redbeds (in dark red) were regionally deposited southward between the Pan African Mountains surrounding the CB. (B) Carboniferous-Permian glacial and deglaciation sequences (in dark grey) derived from west-facing paleo-valleys incised along the eastern margin of the basin. These sequences possibly connected with the Karoo and Paraná Seas of southwestern Gondwana. (C) Triassic fluvial (aeolian?) red sandstones and siltstones (in brown) were deposited across the entire CB; but outcrops are poorly described. (D) Upper Jurassic-Lower Cretaceous fluvial-delta and aeolian sequences (in pink and pale red respectively) record a short marine transgression (from the proto-Indian Ocean) in the northeastern CB, and a paleo-desert in the southern part of the basin extending to Namibia and South America. Strong wind systems were blowing to the southwest at low latitudes across interior Gondwana. (E) Mid- Upper Cretaceous lake sequences (in green) and Cenozoic alluviums (in yellow) derived from the south, possibly related to marginal uplifts of the CB and the Kalahari epeirogeny of southern Africa.

Figure 8: Cross-section across western Gondwana (Fig. 7D for location) showing a Central Gondwana Basin flanked along its southern convergent margin by the proto-Andes. Prevailing near-surface paleo-wind directions were to the south, whilst delicate Permian-Jurassic detrital zircons originating from volcanoes along the proto-Andes imply high atmospheric flow regimes to the north into the interior of Gondwana (arrows).

Tables

Table 1: U-Pb results of detrital zircons from sample D1853 (the Inkisi Group).

Table 2: U-Pb results of detrital zircons from sample D1595 (the Lower Lukuga Group).

Table 3: U-Pb results of detrital zircons from sample D1400 (the Upper Lukuga Group).

Table 4: U-Pb results of detrital zircons from sample S2035 (the Haute Lueki Group).

Table 5: U-Pb results of detrital zircons from sample S1605 (the Haute Lueki Group).

Table 6: U-Pb results of detrital zircons from sample D600 (the Lower Kwango Group).

Table 7: U-Pb results of detrital zircons from sample D470 (the Lower Kwango Group).

Table 8: U-Pb results of detrital zircons from sample WP19 (the Lower Kwango Group).

Table 9: U-Pb results of detrital zircons from sample WP103 (the Kalahari Group).

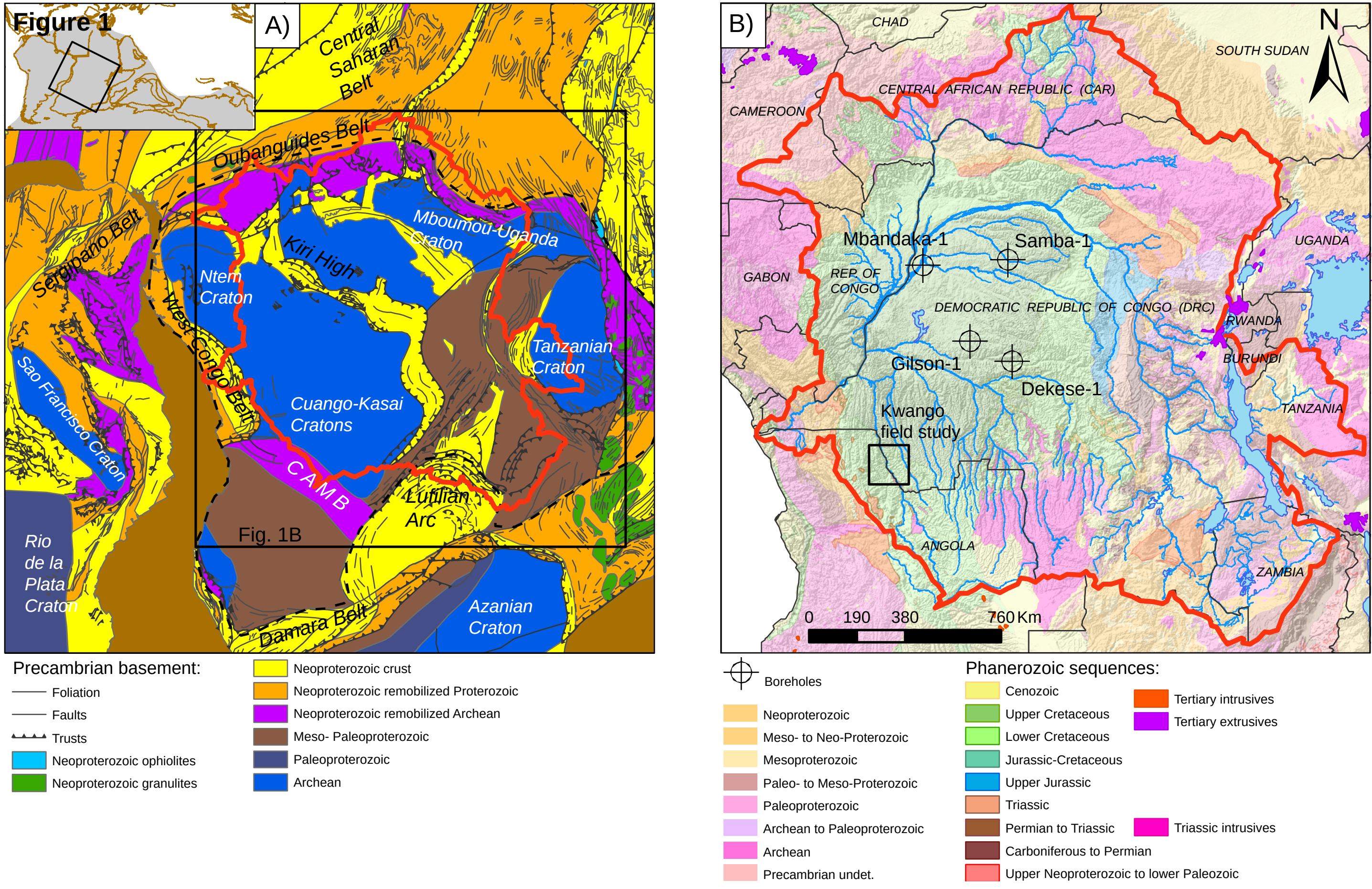
Figure 1
A)
Central Saharan Belt
Oubanguides Belt
Sergipano Belt
Ntem Craton
Kiri High
Mboumou-Uganda Craton
West Congo Belt
Tanzanian Craton
Sao Francisco Craton
Cuango-Kasai Cratons
CAMB
Lufilian Arc
Fig. 1B
Rio de la Plata Craton
Damara Belt
Azanian Craton
Precambrian basement:
Foliation
Faults
Trusts
Neoproterozoic ophiolites
Neoproterozoic granulites
Neoproterozoic crust
Neoproterozoic remobilized Proterozoic
Neoproterozoic remobilized Archean
Meso- Paleoproterozoic
Paleoproterozoic
Archean
B)
N
CHAD
SOUTH SUDAN
CENTRAL AFRICAN REPUBLIC (CAR)
CAMEROON
UGANDA
GABON
REP OF CONGO
DEMOCRATIC REPUBLIC OF CONGO (DRC)
RWANDA
BURUNDI
TANZANIA
ANGOLA
ZAMBIA
Mbandaka-1
Samba-1
Gilson-1
Dekese-1
Kwango field study
0 190 380 760 Km
Boreholes
Neoproterozoic
Meso- to Neo-Proterozoic
Mesoproterozoic
Paleo- to Meso-Proterozoic
Paleoproterozoic
Archean to Paleoproterozoic
Archean
Precambrian undet.
Phanerozoic sequences:
Cenozoic
Upper Cretaceous
Lower Cretaceous
Jurassic-Cretaceous
Upper Jurassic
Triassic
Permian to Triassic
Carboniferous to Permian
Upper Neoproterozoic to lower Paleozoic
Tertiary intrusives
Tertiary extrusives
Triassic intrusives

Figure 2

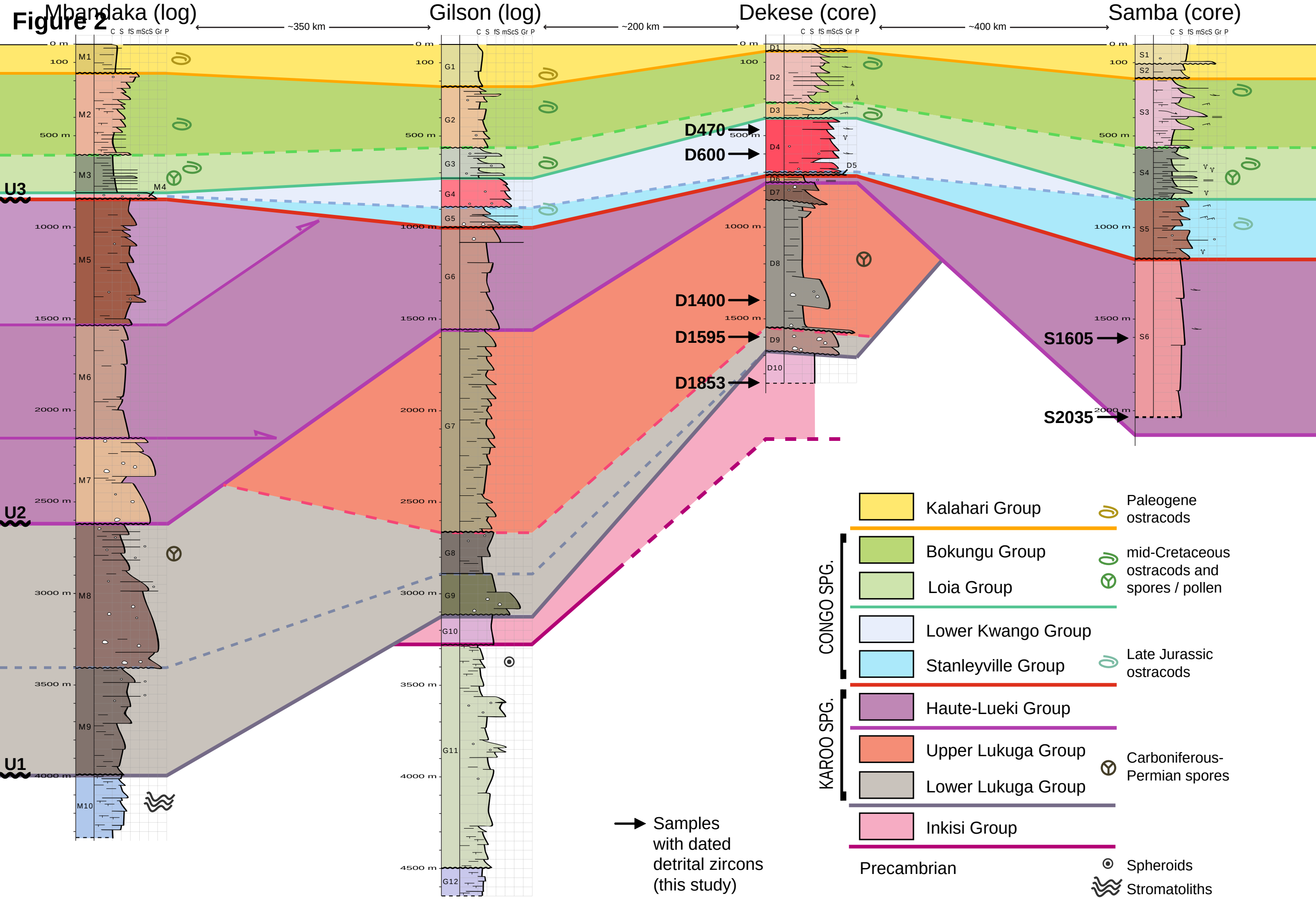

Mbandaka (log)
Gilson (log)
Dekese (core)
Samba (core)
~350 km
~200 km
~400 km
C S fS mScS Gr P
U3
U2
U1
D470
D600
D1400
D1595
D1853
S1605
S2035
Kalahari Group
Bokungu Group
Loia Group
Lower Kwango Group
Stanleyville Group
Haute-Lueki Group
Upper Lukuga Group
Lower Lukuga Group
Inkisi Group
Precambrian
CONGO SPG.
KAROO SPG.
Paleogene ostracods
mid-Cretaceous ostracods and spores / pollen
Late Jurassic ostracods
Carboniferous-Permian spores
Spheroids
Stromatoliths
Samples with dated detrital zircons (this study)

Figure 3

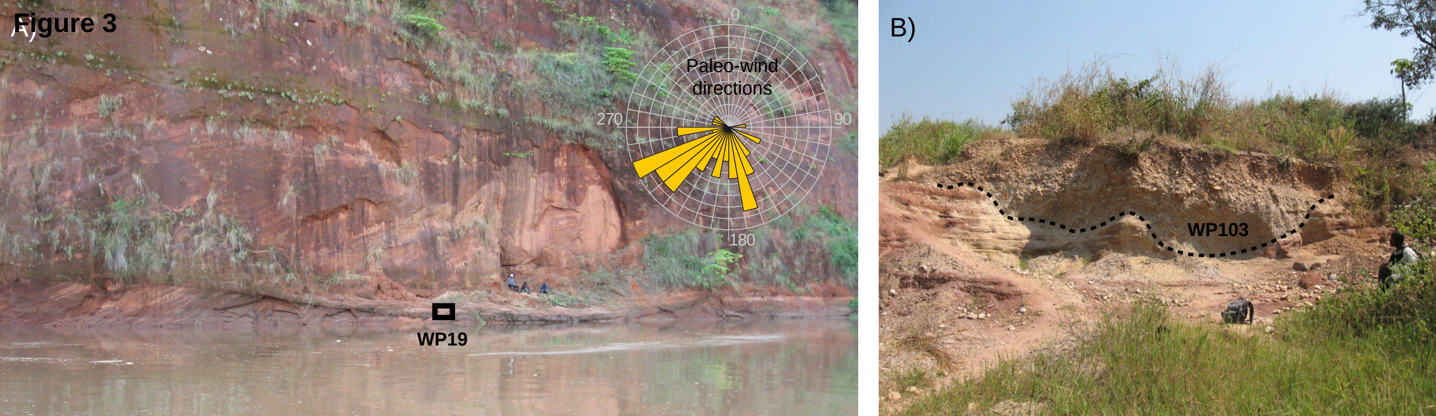

Figure 4

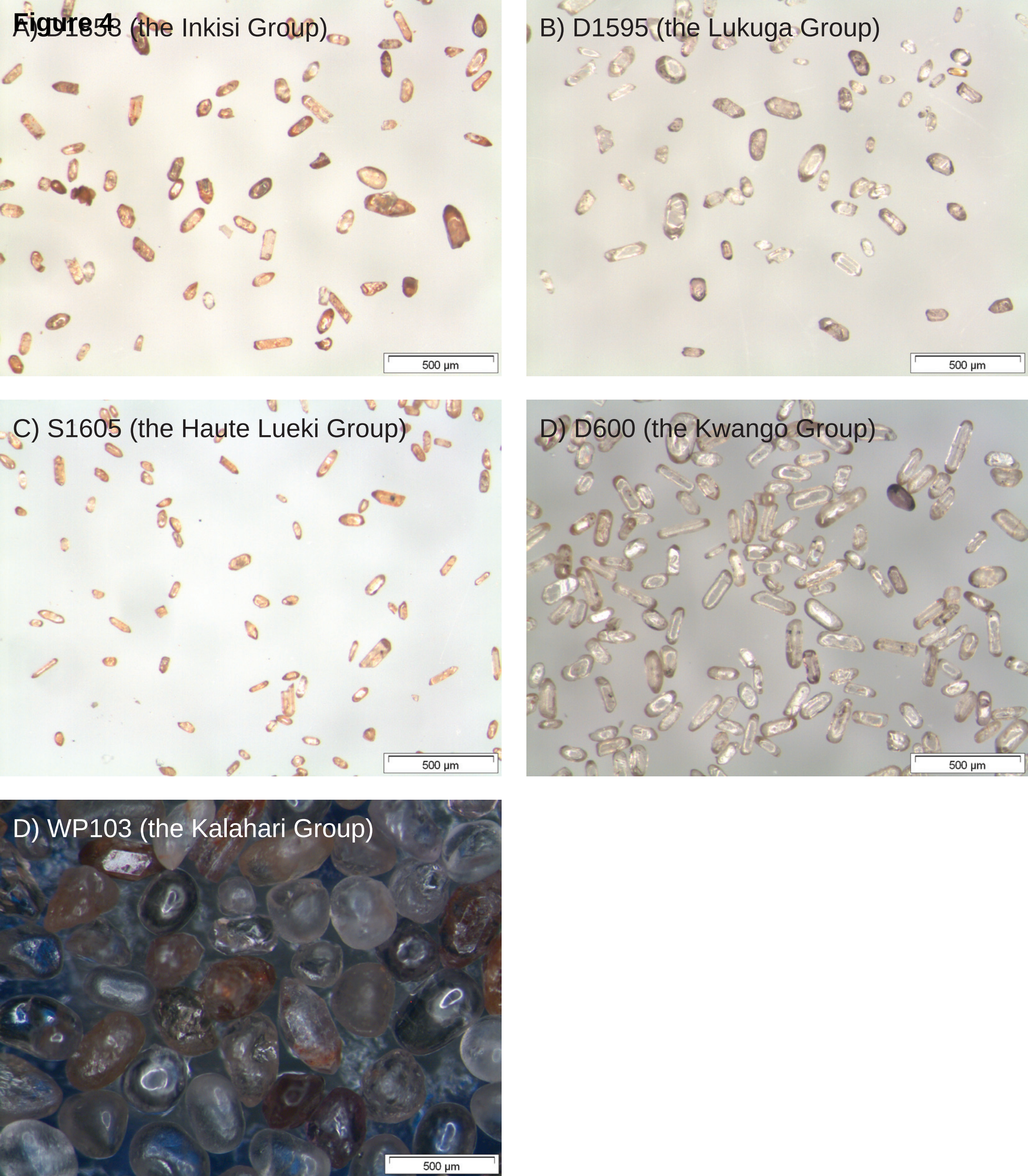
A) D1853 (the Inkisi Group)
500 µm
B) D1595 (the Lukuga Group)
500 µm
C) S1605 (the Haute Lueki Group)
500 µm
D) D600 (the Kwango Group)
500 µm
D) WP103 (the Kalahari Group)
500 µm

Figure 5

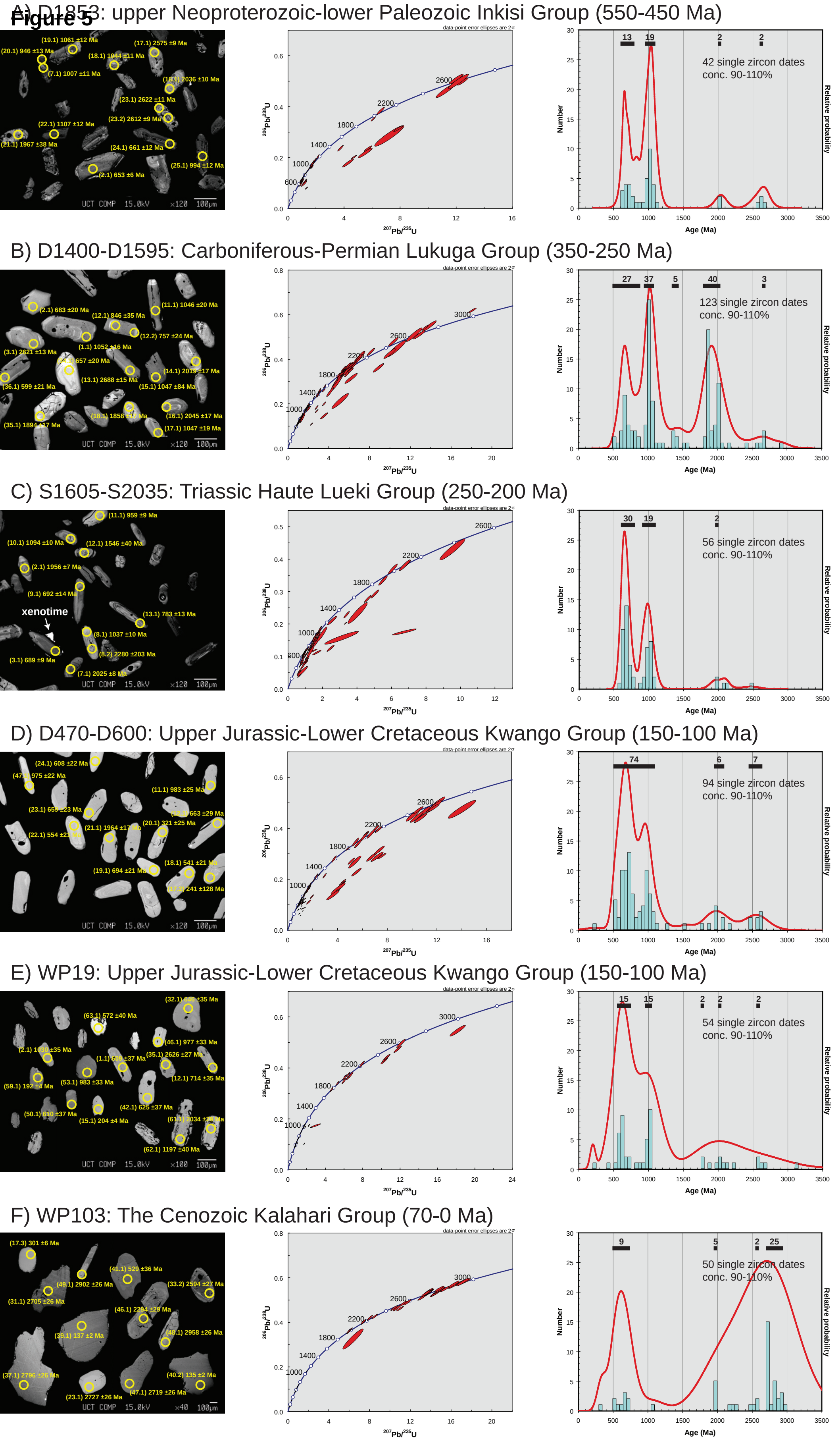
A) D1853: upper Neoproterozoic-lower Paleozoic Inkisi Group (550-450 Ma)
42 single zircon dates
conc. 90-110%
B) D1400-D1595: Carboniferous-Permian Lukuga Group (350-250 Ma)
123 single zircon dates
conc. 90-110%
C) S1605-S2035: Triassic Haute Lueki Group (250-200 Ma)
xenotime
56 single zircon dates
conc. 90-110%
D) D470-D600: Upper Jurassic-Lower Cretaceous Kwango Group (150-100 Ma)
94 single zircon dates
conc. 90-110%
E) WP19: Upper Jurassic-Lower Cretaceous Kwango Group (150-100 Ma)
54 single zircon dates
conc. 90-110%
F) WP103: The Cenozoic Kalahari Group (70-0 Ma)
50 single zircon dates
conc. 90-110%
data-point error ellipses are 2σ
$^{206}Pb/^{238}U$
$^{207}Pb/^{235}U$
Number
Age (Ma)
Relative probability
UCT COMP 15.0kV

Figure 6

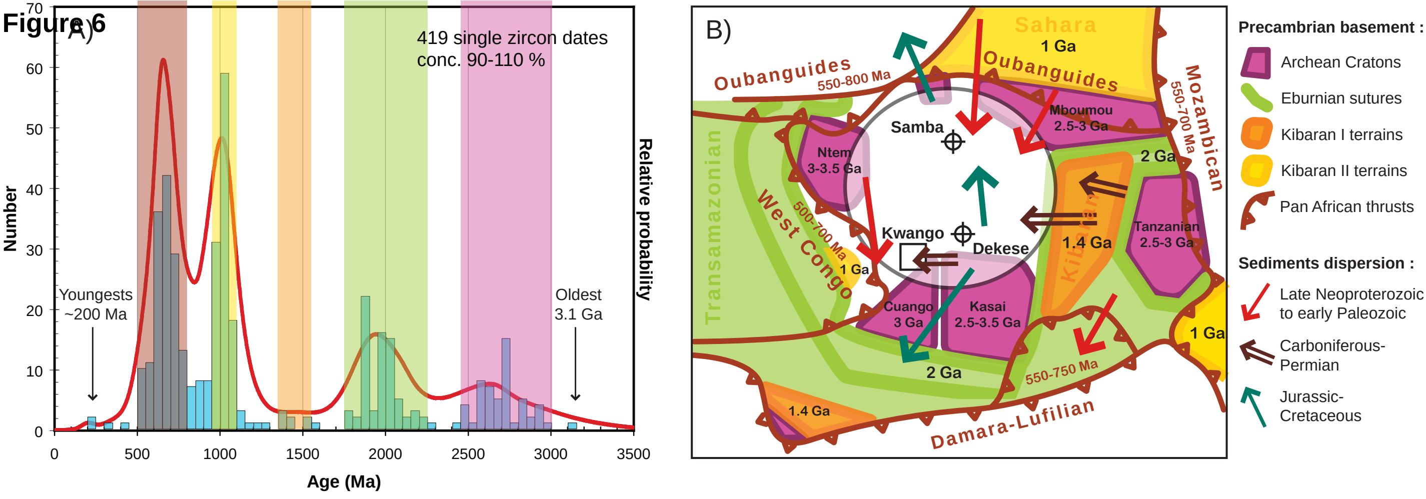

A)
419 single zircon dates
conc. 90-110 %
Number
Relative probability
Age (Ma)
Youngests
~200 Ma
Oldest
3.1 Ga
0
500
1000
1500
2000
2500
3000
3500
0
10
20
30
40
50
60
70
B)
Sahara
1 Ga
Oubanguides
550-800 Ma
Oubanguides
Mozambican
550-700 Ma
Mboumou
2.5-3 Ga
Samba
Ntem
3-3.5 Ga
2 Ga
Transamazonian
West Congo
500-700 Ma
Kwango
Dekese
1 Ga
1.4 Ga
Kibaran
Tanzanian
2.5-3 Ga
Cuango
3 Ga
Kasai
2.5-3.5 Ga
1 Ga
2 Ga
550-750 Ma
1.4 Ga
Damara-Lufilian
Precambrian basement :
Archean Cratons
Eburnian sutures
Kibaran I terrains
Kibaran II terrains
Pan African thrusts
Sediments dispersion :
Late Neoproterozoic
to early Paleozoic
Carboniferous-
Permian
Jurassic-
Cretaceous

Figure 7

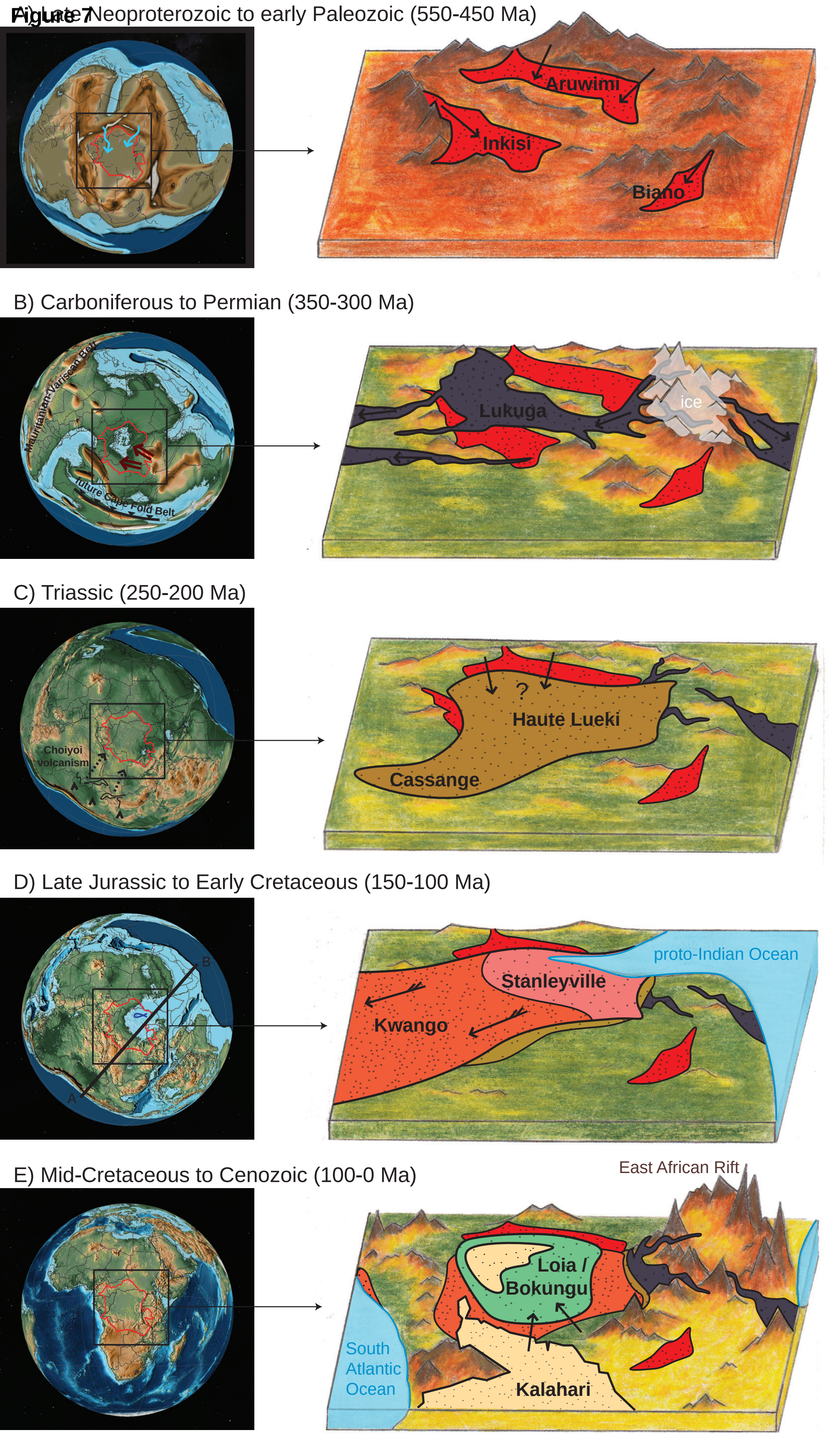
A) Late Neoproterozoic to early Paleozoic (550-450 Ma)
Aruwimi
Inkisi
Biano
B) Carboniferous to Permian (350-300 Ma)
Mauritanian-Variscan Belt
future Cape Fold Belt
Lukuga
ice
C) Triassic (250-200 Ma)
Choiyoi volcanism
?
Haute Lueki
Cassange
D) Late Jurassic to Early Cretaceous (150-100 Ma)
B
A
proto-Indian Ocean
Stanleyville
Kwango
E) Mid-Cretaceous to Cenozoic (100-0 Ma)
East African Rift
Loia / Bokungu
South Atlantic Ocean
Kalahari

Figure 8

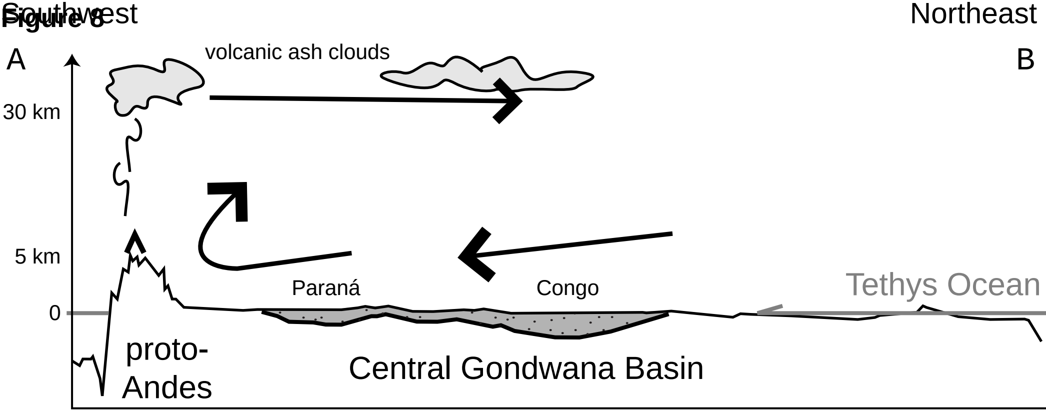
Southwest
Northeast
A
B
volcanic ash clouds
30 km
5 km
0
Paraná
Congo
Tethys Ocean
proto-Andes
Central Gondwana Basin

Table 1

sample	spot Ø	U [ppm]	Pb [ppm]	ratios $^{207}Pb/^{206}Pb$	1σ	$^{207}Pb/^{235}U$	1σ	$^{206}Pb/^{238}U$	1σ	$^{207}Pb/^{206}Pb$	2σ	$^{207}Pb/^{235}U$	2σ	$^{206}Pb/^{238}U$	2σ	conc.
D11 L_1.1_10-35-55	35	2	0	0.083489	3.96	1.195708	5.18	0.10387	3.33	1281	77	799	58	637	41	50
D11 L_2.1_10-35-55	35	288	27	0.061395	0.29	0.929508	1.17	0.10980	1.14	653	6	667	12	672	14	103
D11 L_3.1_10-35-55	35	217	34	0.074285	0.31	1.834944	0.83	0.17915	0.77	1049	6	1058	11	1062	15	101
D11 L_4.1_10-35-55	35	240	77	0.125846	0.40	6.093347	1.09	0.35117	1.01	2041	7	1989	19	1940	34	95
D11 L_5.1_10-35-55	35	167	15	0.061223	0.37	0.853262	0.93	0.10108	0.85	647	8	626	9	621	10	96
D11 L_6.1_10-35-55	35	204	25	0.066915	0.37	1.271852	1.01	0.13785	0.93	835	8	833	11	833	15	100
D11 L_7.1_10-35-55	35	405	42	0.063040	0.32	1.025571	0.99	0.11799	0.94	710	7	717	10	719	13	101
D11 L_8.1_10-35-55	35	269	41	0.074121	0.31	1.747181	0.91	0.17096	0.86	1045	6	1026	12	1017	16	97
D11 L_9.1_10-35-55	35	826	120	0.075064	0.44	1.666577	1.20	0.16103	1.12	1070	9	996	15	962	20	90
D11 L_10.1_10-35-55	35	796	62	0.064085	1.15	0.773519	1.38	0.08754	0.77	744	24	582	12	541	8	73
D11 L_11.1_10-35-55	35	151	77	0.181952	0.29	12.490581	1.24	0.49788	1.21	2671	5	2642	23	2605	52	98
D11 L_12.1_10-25-55	25	195	29	0.073562	0.56	1.760987	1.82	0.17362	1.73	1029	11	1031	24	1032	33	100
D11 L_13.1_10-25-55	25	43	18	0.176928	0.56	11.267724	2.50	0.46189	2.44	2624	9	2546	47	2448	100	93
D11 L_14.1_10-25-55	25	490	98	0.115437	1.00	3.748952	2.22	0.23554	1.98	1887	18	1582	36	1363	49	72
D11 L_15.1_10-25-55	25	821	115	0.076937	0.81	1.725214	1.69	0.16263	1.48	1120	16	1018	22	971	27	87
D11 L_16.1_10-25-55	25	493	168	0.125527	0.59	6.618316	1.67	0.38239	1.57	2036	10	2062	30	2087	56	103
D11 L_17.1_10-25-55	25	263	125	0.171726	0.51	12.013340	1.67	0.50737	1.59	2575	9	2605	32	2645	69	103
D11 L_18.1_10-25-55	25	440	68	0.074093	0.56	1.850553	1.73	0.18114	1.63	1044	11	1064	23	1073	32	103
D11 L_19.1_10-25-55	25	186	29	0.074721	0.59	1.914965	2.29	0.18587	2.21	1061	12	1086	31	1099	45	104
D11 L_20.1_10-25-55	25	56	8	0.070600	0.62	1.676111	1.73	0.17219	1.62	946	13	1000	22	1024	31	108
D11 L_20.2_10-25-55	25	335	48	0.072755	0.56	1.691224	1.61	0.16859	1.51	1007	11	1005	21	1004	28	100
D11 L_21.1_10-25-55	25	1110	77	0.120742	2.13	1.311818	3.39	0.07880	2.64	1967	38	851	39	489	25	25
D11 L_22.1_10-25-55	25	58	10	0.076438	0.60	2.124907	1.98	0.20162	1.89	1107	12	1157	28	1184	41	107
D11 L_23.1_10-25-55	25	1098	245	0.176695	0.66	5.706987	2.02	0.23425	1.91	2622	11	1932	35	1357	47	52
D11 L_23.2_10-25-55	25	1819	299	0.175645	0.56	4.295603	3.74	0.17737	3.70	2612	9	1693	63	1053	72	40
D11 L_24.1_10-25-55	25	191	18	0.061629	0.58	0.934118	1.82	0.10993	1.72	661	12	670	18	672	22	102
D11 L_25.1_10-25-55	25	86	13	0.072303	0.58	1.736777	2.11	0.17421	2.03	994	12	1022	27	1035	39	104
D11 L_26.1_10-25-55	25	572	48	0.068612	4.40	0.940815	4.86	0.09945	2.07	887	91	673	48	611	24	69
D11 L_27.1_10-25-55	25	288	45	0.072089	0.53	1.763349	2.13	0.17741	2.06	988	11	1032	28	1053	40	107
D11 L_28.1_10-25-55	25	584	54	0.070794	0.84	1.068269	2.94	0.10944	2.82	951	17	738	31	670	36	70
D11 L_29.1_10-25-55	25	360	34	0.063939	1.79	0.966155	2.51	0.10959	1.75	740	38	686	25	670	22	91
D11 L_30.1_10-25-55	25	1708	454	0.184534	0.61	7.235245	5.93	0.28436	5.89	2694	10	2141	109	1613	169	60
D11 S_1.1_10-25-55	25	291	28	0.062530	0.61	0.961700	1.54	0.11155	1.42	692	13	684	15	682	18	98
D11 S_2.1_10-25-55	25	290	42	0.070956	0.64	1.606576	1.73	0.16422	1.60	956	13	973	22	980	29	103
D11 S_3.1_10-25-55	25	190	28	0.074328	1.10	1.710133	2.21	0.16687	1.92	1050	22	1012	29	995	35	95
D11 S_4.1_10-25-55	25	259	24	0.060671	0.58	0.896927	1.89	0.10722	1.80	628	13	650	18	657	23	105
D11 S_5.1_10-25-55	25	343	42	0.068411	0.97	1.343863	1.73	0.14247	1.43	881	20	865	20	859	23	97
D11 S_6.1_10-25-55	25	70	11	0.074227	0.73	1.829605	1.82	0.17877	1.67	1048	15	1056	24	1060	33	101
D11 S_7.1_10-25-55	25	502	51	0.062955	0.71	1.009572	1.63	0.11631	1.47	707	15	709	17	709	20	100
D11 S_8.1_10-25-55	25	198	22	0.065017	0.56	1.127694	1.77	0.12580	1.67	775	12	767	19	764	24	99
D11 S_9.1_10-25-55	25	491	70	0.073629	0.86	1.644191	1.72	0.16196	1.49	1031	17	987	22	968	27	94
D11 S_10.1_10-25-55	25	119	11	0.065225	1.03	0.940255	1.73	0.10455	1.40	782	22	673	17	641	17	82
D11 S_11.1_10-25-55	25	311	30	0.061755	0.71	0.924913	1.61	0.10862	1.45	666	15	665	16	665	18	100
D11 S_12.1_10-25-55	25	104	16	0.074319	0.87	1.756150	2.03	0.17138	1.83	1050	17	1029	26	1020	35	97
D11 S_13.1_10-25-55	25	90	8	0.060140	0.97	0.893960	2.56	0.10781	2.37	609	21	648	25	660	30	108
D11 S_14.1_10-25-55	25	219	32	0.070785	0.57	1.642160	1.94	0.16826	1.85	951	12	987	25	1003	34	105
D11 S_15.1_10-25-55	25	52	8	0.073656	0.75	1.896507	1.99	0.18674	1.84	1032	15	1080	27	1104	37	107
D11 S_16.1_10-25-55	25	371	57	0.073437	0.61	1.762692	1.64	0.17409	1.53	1026	12	1032	21	1035	29	101
D11 S_17.1_10-25-55	25	621	49	0.071136	1.44	0.924739	4.07	0.09428	3.81	961	29	665	40	581	42	60
D11 S_18.1_10-25-55	25	175	28	0.074311	0.76	1.812840	1.76	0.17693	1.59	1050	15	1050	23	1050	31	100
D11 S_19.1_10-25-55	25	967	200	0.184456	0.61	5.516352	3.66	0.21690	3.61	2693	10	1903	64	1265	83	47
D11 S_20.1_10-25-55	25	419	33	0.086354	5.23	1.145617	6.84	0.09622	4.41	1346	101	775	76	592	50	44
D11 S_21.1_10-25-55	25	534	49	0.069455	0.77	0.987241	1.68	0.10309	1.50	912	16	697	17	632	18	69
D11 S_22.1_10-25-55	25	431	38	0.066068	1.59	0.910583	2.29	0.09996	1.65	809	33	657	22	614	19	76
D11 S_23.1_10-25-55	25	482	147	0.182898	0.78	7.865586	1.65	0.31190	1.46	2679	13	2216	30	1750	45	65
D11 S_24.1_10-25-55	25	516	50	0.066339	1.33	1.007969	2.67	0.11020	2.32	817	28	708	27	674	30	82
D11 S_25.1_10-25-55	25	542	55	0.082468	0.76	1.271270	1.52	0.11180	1.32	1257	15	833	17	683	17	54
D11 S_26.1_10-25-55	25	122	17	0.070250	0.65	1.500763	1.79	0.15494	1.67	936	13	931	22	929	29	99
D11 S_27.1_10-25-55	25	596	59	0.063871	0.96	0.983693	1.88	0.11170	1.62	737	20	695	19	683	21	93
D11 S_28.1_10-25-55	25	44	7	0.072340	0.65	1.723921	2.90	0.17284	2.83	996	13	1017	38	1028	54	103
D11 S_29.1_10-25-55	25	355	41	0.065575	0.70	1.200736	1.82	0.13280	1.68	793	15	801	20	804	25	101
D11 S_30.1_10-25-55	25	178	86	0.177166	0.59	12.171414	2.42	0.49826	2.35	2627	10	2618	46	2606	101	99
D11 S_30.2_10-25-55	25	616	121	0.170312	0.77	4.711967	1.68	0.20066	1.49	2561	13	1769	28	1179	32	46

Table 2

sample	spot Ø	U [ppm]	Pb [ppm]	ratios $^{207}Pb/^{206}Pb$	1σ	$^{207}Pb/^{235}U$	1σ	$^{206}Pb/^{238}U$	1σ	$^{207}Pb/^{206}Pb$	2σ	$^{207}Pb/^{235}U$	2σ	$^{206}Pb/^{238}U$	2σ	conc.
D9 L_1.1_10-35-55	35	108	18	0.074401	0.78	1.916965	2.72	0.18687	2.61	1052	16	1087	37	1104	53	105
D9 L_2.1_10-35-55	35	185	18	0.062257	0.93	0.965333	2.63	0.11246	2.47	683	20	686	26	687	32	101
D9 L_3.1_10-35-55	35	169	82	0.176601	0.78	12.401141	2.60	0.50929	2.48	2621	13	2635	49	2654	108	101
D9 L_4.1_10-35-55	35	64	20	0.115141	0.79	5.370031	2.62	0.33826	2.49	1882	14	1880	45	1878	82	100
D9 L_5.1_10-35-55	35	180	57	0.114137	0.82	5.481889	2.71	0.34834	2.58	1866	15	1898	47	1927	86	103
D9 L_6.1_10-35-55	35	51	8	0.075506	0.87	1.877232	2.61	0.18032	2.46	1082	17	1073	35	1069	48	99
D9 L_7.1_10-35-55	35	118	12	0.062478	0.99	1.005639	2.93	0.11674	2.76	691	21	707	30	712	37	103
D9 L_8.1_10-35-55	35	249	23	0.060520	0.85	0.896393	2.63	0.10742	2.48	622	18	650	25	658	31	106
D9 L_8.2_10-35-55	35	577	55	0.061344	0.85	0.931635	2.56	0.11015	2.41	651	18	668	25	674	31	103
D9 L_9.1_10-35-55	35	142	13	0.065371	1.15	0.966952	2.90	0.10728	2.66	786	24	687	29	657	33	84
D9 L_10.1_10-25-55	25	147	23	0.074161	0.96	1.823084	1.96	0.17829	1.71	1046	19	1054	26	1058	33	101
D9 L_11.1_10-25-55	25	39	6	0.074179	1.00	1.821866	1.88	0.17813	1.59	1046	20	1053	25	1057	31	101
D9 L_12.1_10-25-55	25	77	9	0.067264	1.69	1.165765	2.49	0.12570	1.83	846	35	785	27	763	26	90
D9 L_12.2_10-15-55	25	81	9	0.064467	1.14	1.190333	2.51	0.13391	2.24	757	24	796	28	810	34	107
D9 L_13.1_10-25-55	25	171	85	0.183889	0.93	12.898897	1.82	0.50874	1.57	2688	15	2672	35	2651	68	99
D9 L_14.1_10-25-55	25	398	150	0.124333	0.94	6.920386	2.08	0.40368	1.85	2019	17	2101	37	2186	69	108
D9 L_15.1_10-25-55	25	58	7	0.074214	4.15	1.360778	4.56	0.13298	1.89	1047	84	872	54	805	29	77
D9 L_16.1_10-25-55	25	236	86	0.126160	0.96	6.830598	1.93	0.39268	1.68	2045	17	2090	34	2135	61	104
D9 L_17.1_10-25-55	25	97	16	0.074205	0.95	1.839339	1.82	0.17977	1.55	1047	19	1060	24	1066	30	102
D9 L_18.1_10-25-55	25	227	68	0.113602	0.95	5.078570	1.95	0.32423	1.70	1858	17	1833	33	1810	54	97
D9 L_19.1_10-25-55	25	109	17	0.071224	0.96	1.719401	1.93	0.17509	1.68	964	20	1016	25	1040	32	108
D9 L_20.1_10-25-55	25	141	45	0.114982	0.96	5.524330	1.85	0.34846	1.58	1880	17	1904	32	1927	53	103
D9 L_21.1_10-25-55	25	80	25	0.115614	0.97	5.350290	2.09	0.33563	1.85	1889	17	1877	36	1866	60	99
D9 L_22.1_10-25-55	25	100	31	0.115340	0.96	5.385322	2.06	0.33863	1.82	1885	17	1883	36	1880	60	100
D9 L_23.1_10-25-55	25	163	52	0.114842	0.94	5.337474	1.86	0.33708	1.60	1877	17	1875	32	1873	52	100
D9 L_24.1_10-25-55	25	694	81	0.076940	1.38	1.452036	5.66	0.13688	5.49	1120	28	911	69	827	85	74
D9 L_25.1_10-25-55	25	235	52	0.087508	0.96	2.928560	1.95	0.24272	1.69	1372	19	1389	30	1401	43	102
D9 L_26.1_10-25-55	25	450	42	0.062958	1.01	0.904598	1.87	0.10421	1.57	707	22	654	18	639	19	90
D9 L_27.1_10-25-55	25	128	40	0.116163	0.95	5.382189	1.83	0.33604	1.56	1898	17	1882	32	1868	51	98
D9 L_28.1_10-25-55	25	647	231	0.178750	0.99	8.882398	2.40	0.36040	2.18	2641	16	2326	44	1984	75	75
D9 L_29.1_10-25-55	25	176	28	0.073853	0.95	1.777801	1.88	0.17459	1.62	1037	19	1037	25	1037	31	100
D9 L_30.1_10-25-55	25	1549	295	0.129514	0.99	3.550961	2.03	0.19885	1.77	2091	17	1539	32	1169	38	56
D9 L_31.1_10-25-55	25	301	125	0.170864	1.00	10.024796	2.52	0.42552	2.32	2566	17	2437	47	2286	90	89
D9 L_32.1_10-25-55	25	127	30	0.088917	0.95	3.099945	1.83	0.25285	1.56	1402	18	1433	28	1453	41	104
D9 L_33.1_10-25-55	25	61	7	0.069118	1.29	1.188354	3.36	0.12470	3.11	902	27	795	37	758	44	84
D9 L_34.1_10-25-55	25	522	50	0.061516	0.95	0.911840	1.82	0.10750	1.56	657	20	658	18	658	20	100
D9 L_35.1_10-20-55	20	260	88	0.115926	0.94	5.836804	2.22	0.36517	2.01	1894	17	1952	39	2007	70	106
D9 L_36.1_10-25-55	25	367	32	0.059862	0.95	0.799291	1.86	0.09684	1.60	599	21	596	17	596	18	100
D9 L_37.1_10-25-55	25	2858	304	0.155640	1.09	2.317478	2.33	0.10799	2.07	2409	18	1218	33	661	26	27
D9 L_38.1_10-25-55	25	276	47	0.075958	0.96	1.938536	1.94	0.18510	1.68	1094	19	1094	26	1095	34	100
D9 L_39.1_10-25-55	25	17	3	0.073318	1.18	1.771088	2.23	0.17520	1.89	1023	24	1035	29	1041	36	102
D9 L_40.1_10-25-55	25	214	33	0.072623	0.96	1.699721	1.80	0.16975	1.52	1003	19	1008	23	1011	29	101
D9 L_41.1_10-25-55	25	86	10	0.064740	1.05	1.092091	2.11	0.12235	1.83	766	22	750	23	744	26	97
D9 L_42.1_10-25-55	25	1079	170	0.123430	0.96	2.819881	2.12	0.16569	1.89	2006	17	1361	32	988	35	49
D9 L_43.1_10-25-55	25	125	20	0.074645	0.97	1.774429	1.82	0.17241	1.53	1059	20	1036	24	1025	29	97
D9 L_43.2_10-20-55	20	157	13	0.060978	1.01	0.767414	2.40	0.09128	2.17	638	22	578	21	563	23	88
D9 S_1.1_10-25-55	25	144	16	0.070309	0.66	1.259615	1.37	0.12994	1.20	937	13	828	16	787	18	84
D9 S_2.1_10-25-55	25	288	96	0.124771	0.56	6.371121	1.36	0.37034	1.24	2026	10	2028	24	2031	43	100
D9 S_3.1_10-25-55	25	678	111	0.111793	0.63	2.810227	2.21	0.18232	2.12	1829	11	1358	33	1080	42	59
D9 S_4.1_10-25-55	25	403	44	0.064860	0.61	1.130127	1.39	0.12637	1.25	770	13	768	15	767	18	100
D9 S_5.1_10-25-55	25	837	279	0.119931	0.58	6.122039	1.41	0.37022	1.29	1955	10	1993	25	2030	45	104
D9 S_5.2_10-25-55	51	108	31	0.143772	2.75	6.207907	4.07	0.31316	3.01	2273	47	2006	73	1756	93	77
D9 S_6.1_10-25-55	25	1164	162	0.177948	0.62	3.547098	4.21	0.14457	4.16	2634	10	1538	68	870	68	33
D9 S_7.1_10-25-55	25	283	23	0.060813	0.60	0.807779	1.46	0.09634	1.33	633	13	601	13	593	15	94
D9 S_8.1_10-25-55	25	598	135	0.119474	0.65	4.138960	3.40	0.25126	3.33	1948	12	1662	56	1445	87	74
D9 S_9.1_10-25-55	25	377	110	0.114600	0.55	5.132825	2.43	0.32484	2.36	1874	10	1842	42	1813	75	97
D9 S_10.1_10-25-55	25	642	159	0.094200	0.60	3.604465	1.33	0.27752	1.19	1512	11	1551	21	1579	33	104
D9 S_11.1_10-25-55	25	199	31	0.074666	0.64	1.875596	1.57	0.18219	1.44	1060	13	1073	21	1079	29	102
D9 S_12.1_10-25-55	25	319	37	0.067869	1.20	1.277880	3.04	0.13656	2.79	865	25	836	35	825	43	95
D9 S_13.1_10-25-55	25	140	31	0.088725	0.67	3.043215	1.46	0.24876	1.30	1398	13	1419	22	1432	33	102
D9 S_14.1_10-25-55	25	571	119	0.089781	0.82	2.919313	1.59	0.23583	1.35	1421	16	1387	24	1365	33	96
D9 S_15.1_10-25-55	25	375	37	0.061795	0.60	0.964625	1.74	0.11321	1.63	667	13	686	17	691	21	104
D9 S_16.1_10-25-55	25	134	45	0.126337	0.58	6.498384	1.76	0.37306	1.67	2048	10	2046	31	2044	58	100
D9 S_17.1_10-25-55	25	137	20	0.073414	0.65	1.681034	1.88	0.16607	1.76	1025	13	1001	24	990	32	97
D9 S_18.1_10-25-55	25	158	51	0.115547	0.58	5.510313	1.43	0.34587	1.31	1888	10	1902	25	1915	44	101
D9 S_19.1_10-25-55	25	164	21	0.067805	0.64	1.373909	1.56	0.14696	1.42	863	13	878	18	884	24	102
D9 S_20.1_10-25-55	25	52	16	0.115854	0.62	5.337914	1.39	0.33416	1.25	1893	11	1875	24	1859	40	98
D9 S_21.1_10-25-55	25	226	21	0.061747	0.65	0.905960	1.49	0.10641	1.34	665	14	655	14	652	17	98
D9 S_22.1_10-25-55	25	87	11	0.072731	0.87	1.442632	2.71	0.14386	2.57	1006	18	907	33	866	42	86
D9 S_23.1_10-25-55	25	152	23	0.073904	0.71	1.749056	1.63	0.17165	1.46	1039	14	1027	21	1021	28	98
D9 S_24.1_10-25-55	25	141	43	0.110153	0.65	4.953520	1.59	0.32615	1.45	1802	12	1811	27	1820	46	101
D9 S_25.1_10-25-55	25	257	24	0.061805	0.82	0.896099	1.57	0.10515	1.33	667	18	650	15	645	16	97
D9 S_26.1_10-25-55	34	20	2	0.072572	0.82	1.396325	1.12	0.13955	0.76	1002	17	887	13	842	12	84
D9 S_27.1_10-25-55	35	65	10	0.073196	0.77	1.744601	1.40	0.17286	1.17	1019	16	1025	18	1028	22	101
D9 S_28.1_10-25-55	36	174	17	0.066593	1.56	1.006311	2.53	0.10960	1.99	825	33	707	26	670	25	81
D9 S_29.1_10-25-55	39	107	14	0.067344	0.52	1.425319	1.11	0.15350	0.98	848	11	900	13	921	17	109
D9 S_30.1_10-25-55	40	94	13	0.073848	0.88	1.674467	1.37	0.16445	1.04	1037	18	999	17	981	19	95
D9 S_31.1_10-25-55	43	61	19	0.115313	0.50	5.563258	0.99	0.34990	0.86	1885	9	1910	17	1934	29	103
D9 S_32.1_10-25-55	46	62	7	0.063535	0.47	1.111530	0.94	0.12688	0.82	726	10	759	10	770	12	106
D9 S_33.1_10-25-55	47	34	20	0.212504	0.48	18.116035	0.87	0.61829	0.72	2925	8	2996	17	3103	36	106
D9 S_34.1_10-25-55	48	34	11	0.115304	0.51	5.681283	1.03	0.35736	0.89	1885	9	1929	18	1970	30	105
D9 S_35.1_10-25-55	49	25	4	0.077805	0.55	2.065040	1.09	0.19249	0.94	1142	11	1137	15	1135	20	99
D9 S_36.1_10-25-55	50	48	5	0.062346	0.52	1.053715	0.90	0.12258	0.73	686	11	731	9	745	10	109

Table 3

sample	spot Ø	U [ppm]	Pb [ppm]	ratios $^{207}Pb/^{206}Pb$	1σ	$^{207}Pb/^{235}U$	1σ	$^{206}Pb/^{238}U$	1σ	$^{207}Pb/^{206}Pb$	2σ	$^{207}Pb/^{235}U$	2σ	$^{206}Pb/^{238}U$	2σ	conc.
D8 L_1.1_10-35-55	35	198	20	0.063052	0.74	1.065998	2.67	0.12262	2.57	710	16	737	28	746	36	105
D8 L_2.1_10-35-55	35	176	26	0.073216	0.73	1.764828	2.56	0.17482	2.45	1020	15	1033	33	1039	47	102
D8 L_3.1_10-35-55	35	706	68	0.066101	0.96	1.094903	5.01	0.12013	4.92	810	20	751	54	731	68	90
D8 L_4.1_10-35-55	35	164	26	0.074961	0.74	1.891210	2.75	0.18298	2.65	1067	15	1078	37	1083	53	101
D8 L_5.1_10-35-55	35	34	6	0.074817	0.80	1.962046	2.68	0.19020	2.55	1064	16	1103	36	1122	53	106
D8 L_6.1_10-35-55	35	183	68	0.125742	1.02	7.110912	2.62	0.41015	2.42	2039	18	2125	47	2216	91	109
D8 L_6.2_10-35-55	35	254	80	0.120812	0.73	5.764138	2.53	0.34604	2.42	1968	13	1941	44	1916	80	97
D8 L_7.1_10-35-55	35	63	10	0.073664	0.79	1.799031	2.63	0.17713	2.51	1032	16	1045	35	1051	49	102
D8 L_8.1_10-35-55	35	90	14	0.072854	0.78	1.754719	2.59	0.17469	2.47	1010	16	1029	34	1038	47	103
D8 L_9.1_10-35-55	35	319	114	0.123711	0.73	6.782288	2.56	0.39762	2.45	2010	13	2083	46	2158	90	107
D8 L_10.1_10-25-55	25	517	202	0.136585	0.93	8.127245	1.85	0.43156	1.60	2184	16	2245	34	2313	62	106
D8 L_11.1_10-25-55	25	648	145	0.086446	0.94	3.080761	1.76	0.25847	1.48	1348	18	1428	27	1482	39	110
D8 L_11.2_10-25-55	25	711	145	0.087472	0.94	2.879710	1.97	0.23877	1.73	1371	18	1377	30	1380	43	101
D8 L_12.1_10-25-55	25	538	41	0.058375	0.95	0.734784	1.88	0.09129	1.62	544	21	559	16	563	18	104
D8 L_13.1_10-25-55	25	521	178	0.125729	0.94	6.616784	1.99	0.38169	1.76	2039	17	2062	35	2084	63	102
D8 L_14.1_10-25-55	25	159	24	0.072425	0.95	1.697641	2.45	0.17000	2.26	998	19	1008	32	1012	42	101
D8 L_15.1_10-25-55	25	520	186	0.125643	0.94	6.859309	1.85	0.39595	1.60	2038	17	2093	33	2150	58	106
D8 L_16.1_10-25-55	25	198	62	0.114618	0.96	5.639805	1.95	0.35687	1.69	1874	17	1922	34	1967	58	105
D8 L_17.1_10-25-55	25	235	35	0.074025	1.03	1.766760	1.87	0.17310	1.56	1042	21	1033	24	1029	30	99
D8 L_18.1_10-25-55	25	51	16	0.111708	1.11	5.455737	2.07	0.35422	1.75	1827	20	1894	36	1955	59	107
D8 L_19.1_10-25-55	25	467	134	0.117262	1.21	5.081665	2.60	0.31430	2.30	1915	22	1833	45	1762	71	92
D8 L_20.1_10-25-55	25	173	24	0.074205	0.95	1.686175	2.16	0.16480	1.94	1047	19	1003	28	983	35	94
D8 L_21.1_10-20-55	20	2429	377	0.082753	2.93	2.009302	4.00	0.17610	2.72	1263	57	1119	55	1046	53	83
D8 L_22.1_10-20-55	20	187	17	0.060036	1.03	0.888892	2.17	0.10738	1.91	605	22	646	21	658	24	109
D8 L_23.1_10-20-55	20	1188	503	0.173013	1.12	10.650078	3.54	0.44645	3.35	2587	19	2493	67	2379	134	92
D8 L_24.1_10-25-55	25	283	44	0.073494	0.95	1.851480	1.85	0.18271	1.59	1028	19	1064	25	1082	32	105
D8 L_25.1_10-25-55	25	316	97	0.124810	0.94	6.311598	2.31	0.36677	2.10	2026	17	2020	41	2014	73	99
D8 L_26.1_10-25-55	25	113	17	0.073036	0.97	1.788823	1.95	0.17764	1.69	1015	20	1041	26	1054	33	104
D8 L_27.1_10-20-55	20	1044	401	0.124007	0.93	7.146468	2.01	0.41797	1.78	2015	17	2130	36	2251	68	112
D8 L_28.1_10-25-55	25	92	29	0.114433	0.94	5.438157	1.84	0.34467	1.58	1871	17	1891	32	1909	52	102
D8 L_29.1_10-25-55	25	186	59	0.113215	0.95	5.494212	1.87	0.35197	1.61	1852	17	1900	32	1944	54	105
D8 L_30.1_10-25-55	25	121	64	0.184043	0.97	13.907439	2.01	0.54806	1.76	2690	16	2743	38	2817	81	105
D8 L_31.1_10-25-55	25	183	27	0.071554	0.95	1.694518	1.89	0.17175	1.64	973	19	1006	24	1022	31	105
D8 L_32.1_10-25-55	25	228	77	0.119731	0.95	6.093962	1.87	0.36914	1.61	1952	17	1989	33	2025	56	104
D8 L_33.1_10-25-55	25	477	166	0.123967	0.97	6.431026	1.87	0.37625	1.59	2014	17	2037	33	2059	56	102
D8 L_34.1_10-25-55	25	135	61	0.157399	0.93	10.359344	1.93	0.47734	1.69	2428	16	2467	36	2516	71	104
D8 L_35.1_10-25-55	25	104	16	0.072627	0.97	1.807756	2.03	0.18053	1.78	1004	20	1048	27	1070	35	107
D8 L_36.1_10-20-55	20	2369	651	0.117213	0.98	4.886263	5.09	0.30234	5.00	1914	18	1800	88	1703	150	89
D8 L_36.2_10-20-55	20	1748	422	0.119142	1.15	4.702178	4.65	0.28624	4.51	1943	21	1768	79	1623	130	83
D8 S_1.1_10-25-55	25	592	69	0.065937	0.62	1.198905	1.42	0.13187	1.28	804	13	800	16	799	19	99
D8 S_2.1_10-25-55	25	273	42	0.072905	0.70	1.718169	1.54	0.17093	1.37	1011	14	1015	20	1017	26	101
D8 S_3.1_10-25-55	25	117	19	0.074356	0.71	1.837074	1.36	0.17919	1.16	1051	14	1059	18	1063	23	101
D8 S_4.1_10-25-55	25	269	43	0.073840	0.57	1.812405	1.67	0.17802	1.57	1037	12	1050	22	1056	31	102
D8 S_5.1_10-25-55	25	116	11	0.062917	0.83	0.921552	1.66	0.10623	1.44	705	18	663	16	651	18	92
D8 S_6.1_10-25-55	25	854	234	0.115477	0.57	4.659003	1.74	0.29261	1.64	1887	10	1760	29	1655	48	88
D8 S_7.1_10-25-55	25	504	147	0.126291	0.62	5.922517	2.51	0.34012	2.43	2047	11	1965	44	1887	80	92
D8 S_8.1_10-25-55	25	357	31	0.059433	0.73	0.794290	1.56	0.09693	1.38	583	16	594	14	596	16	102
D8 S_8.2_10-25-55	28	259	22	0.060177	0.52	0.819341	1.09	0.09875	0.96	610	11	608	10	607	11	100
D8 S_9.1_10-25-55	25	172	13	0.058480	0.76	0.689281	1.61	0.08548	1.42	548	17	532	13	529	14	97
D8 S_9.2_10-25-55	25	174	13	0.056465	0.69	0.672614	1.30	0.08639	1.10	471	15	522	11	534	11	113
D8 S_10.1_10-25-55	25	1244	243	0.175855	0.70	5.123771	6.60	0.21132	6.57	2614	12	1840	115	1236	149	47
D8 S_11.1_10-25-55	25	185	63	0.122450	0.61	6.181748	2.03	0.36614	1.93	1992	11	2002	36	2011	67	101
D8 S_12.1_10-25-55	25	138	22	0.072646	0.74	1.752165	1.40	0.17493	1.19	1004	15	1028	18	1039	23	103
D8 S_13.1_10-25-55	25	298	102	0.128240	1.13	6.187195	1.68	0.34992	1.24	2074	20	2003	30	1934	42	93
D8 S_14.1_10-25-55	25	346	55	0.073862	0.59	1.801290	1.96	0.17687	1.87	1038	12	1046	26	1050	36	101
D8 S_15.1_10-25-55	25	731	75	0.074701	0.65	1.414733	7.69	0.13736	7.67	1060	13	895	94	830	120	78
D8 S_16.1_10-25-55	25	206	109	0.180798	0.45	13.468848	0.99	0.54030	0.88	2660	8	2713	19	2785	40	105
D8 S_17.1_10-25-55	25	262	97	0.124109	0.48	6.783776	0.86	0.39643	0.71	2016	8	2084	15	2153	26	107
D8 S_18.1_10-25-55	25	122	29	0.098151	1.49	3.505042	1.96	0.25900	1.27	1589	28	1528	31	1485	34	93
D8 S_19.1_10-25-55	25	62	10	0.079337	1.45	2.020763	1.89	0.18473	1.21	1181	29	1123	26	1093	24	93
D8 S_20.1_10-25-55	25	373	62	0.072883	0.46	1.906534	1.05	0.18972	0.95	1011	9	1083	14	1120	19	111
D8 S_21.1_10-25-55	25	123	39	0.114992	0.51	5.563647	1.87	0.35091	1.80	1880	9	1910	33	1939	61	103
D8 S_22.1_10-25-55	25	312	111	0.119283	0.64	6.221814	1.13	0.37830	0.93	1946	12	2008	20	2068	33	106
D8 S_23.1_10-25-55	25	534	86	0.072382	0.48	1.805946	1.00	0.18096	0.88	997	10	1048	13	1072	17	108
D8 S_24.1_10-25-55	25	417	42	0.061549	0.47	0.989882	1.11	0.11664	1.01	658	10	699	11	711	14	108
D8 S_25.1_10-25-55	25	770	81	0.076518	0.48	1.278319	1.55	0.12116	1.47	1109	10	836	18	737	20	67
D8 S_26.1_10-25-55	25	195	33	0.074055	0.47	1.958900	1.36	0.19185	1.28	1043	10	1102	18	1131	27	108
D8 S_27.1_10-25-55	25	229	37	0.073328	0.48	1.888029	1.11	0.18674	1.00	1023	10	1077	15	1104	20	108
D8 S_28.1_10-25-55	25	130	41	0.114403	0.50	5.516064	1.29	0.34970	1.18	1871	9	1903	22	1933	40	103
D8 S_29.1_10-25-55	25	185	37	0.081576	0.48	2.540312	1.23	0.22585	1.13	1235	9	1284	18	1313	27	106
D8 S_30.1_10-25-55	29	196	24	0.075302	0.79	1.496788	1.74	0.14416	1.55	1077	16	929	21	868	25	81
D8 S_31.1_10-25-55	30	160	48	0.118260	0.46	5.294100	0.88	0.32468	0.75	1930	8	1868	15	1813	24	94
D8 S_32.1_10-25-55	31	35	5	0.073937	0.83	1.690431	1.46	0.16582	1.21	1040	17	1005	19	989	22	95
D8 S_33.1_10-25-55	32	122	40	0.114992	0.46	5.646473	1.31	0.35613	1.22	1880	8	1923	23	1964	41	104

Table 4

sample	spot Ø	U [ppm]	Pb [ppm]	ratios $^{207}Pb/^{206}Pb$	1σ	$^{207}Pb/^{235}U$	1σ	$^{206}Pb/^{238}U$	1σ	$^{207}Pb/^{206}Pb$	2σ	$^{207}Pb/^{235}U$	2σ	$^{206}Pb/^{238}U$	2σ	conc.
S10 L 1.1 10-25-55	25	1548	92	0.090611	1.27	0.876986	6.26	0.07020	6.13	1438	24	639	60	437	52	30
S10 L 1.2 10-25-55	25	1054	149	0.076974	1.60	1.774952	2.39	0.16724	1.78	1121	32	1036	31	997	33	89
S10 L 2.1 10-25-55	25	491	143	0.120003	0.40	5.511502	1.85	0.33310	1.81	1956	7	1902	32	1853	58	95
S10 L 3.1 10-25-55	25	329	31	0.062427	0.43	0.958710	1.39	0.11138	1.33	689	9	683	14	681	17	99
S10 L 3.2 10-20-55	25	61	11	0.280890	3.58	6.749587	4.22	0.17428	2.24	3368	56	2079	76	1036	43	31
S10 L 4.1 10-25-55	25	1399	110	0.081118	0.44	1.029034	1.60	0.09200	1.53	1224	9	718	17	567	17	46
S10 L 5.1 10-25-55	25	295	56	0.088777	3.40	2.567568	4.27	0.20976	2.58	1399	65	1291	63	1228	58	88
S10 L 6.1 10-25-55	25	1197	84	0.066324	0.72	0.756089	1.86	0.08268	1.72	817	15	572	16	512	17	63
S10 L 7.1 10-25-55	25	170	25	0.073387	0.41	1.745827	1.59	0.17254	1.53	1025	8	1026	21	1026	29	100
S10 L 8.1 10-25-55	25	1167	156	0.073844	0.48	1.571251	1.59	0.15432	1.52	1037	10	959	20	925	26	89
S10 L 8.2 10-20-55	25	1321	174	0.144330	11.78	3.111394	12.88	0.15635	5.20	2280	203	1436	208	936	91	41
S10 L 9.1 10-25-55	25	604	54	0.062509	0.65	0.925015	1.62	0.10733	1.48	692	14	665	16	657	19	95
S10 L 10.1 10-25-55	25	611	94	0.075954	0.49	1.875213	1.46	0.17906	1.38	1094	10	1072	19	1062	27	97
S10 L 11.1 10-25-55	25	874	123	0.071042	0.46	1.586280	2.27	0.16194	2.22	959	9	965	28	968	40	101
S10 L 12.1 10-25-55	25	1656	117	0.095904	2.12	1.071488	3.72	0.08103	3.06	1546	40	739	39	502	30	32
S10 L 13.1 10-25-55	25	913	79	0.065281	0.61	0.916682	1.59	0.10184	1.47	783	13	661	16	625	18	80
S10 L 14.1 10-25-55	25	734	103	0.071039	0.38	1.617237	1.43	0.16511	1.37	959	8	977	18	985	25	103
S10 L 15.1 10-25-55	25	602	81	0.070386	0.45	1.512715	1.20	0.15587	1.12	940	9	936	15	934	19	99
S10 L 16.1 10-25-55	25	296	43	0.072672	1.30	1.678859	1.79	0.16755	1.23	1005	26	1001	23	999	23	99
S10 L 16.2 10-25-55	25	627	127	0.108310	0.86	3.397139	2.06	0.22748	1.87	1771	16	1504	33	1321	45	75
S10 L 17.1 10-25-55	25	1669	122	0.069036	0.73	0.826738	2.27	0.08685	2.15	900	15	612	21	537	22	60
S10 L 18.1 10-25-55	25	881	73	0.064348	0.38	0.859518	1.29	0.09688	1.23	753	8	630	12	596	14	79
S10 L 18.2 10-20-55	25	2542	94	0.114913	7.32	0.842923	13.98	0.05320	11.91	1879	132	621	134	334	78	18
S10 L 19.1 10-25-55	25	709	62	0.065639	1.71	0.921313	2.79	0.10180	2.20	795	36	663	27	625	26	79
S10 L 19.2 10-25-55	25	469	40	0.063097	0.65	0.846206	1.69	0.09727	1.56	711	14	623	16	598	18	84
S10 L 20.1 10-25-55	25	839	110	0.070880	0.57	1.472928	1.44	0.15072	1.32	954	12	919	18	905	22	95
S10 L 21.1 10-25-55	25	829	109	0.071597	0.58	1.519822	3.07	0.15396	3.02	974	12	938	38	923	52	95
S10 L 22.1 10-25-55	25	959	65	0.073163	1.81	0.797571	4.68	0.07906	4.32	1018	37	595	43	491	41	48
S10 L 23.1 10-25-55	25	2521	86	0.122222	2.56	0.640217	5.28	0.03799	4.62	1989	46	502	42	240	22	12
S10 S_1.1_10-25-55	25	1465	153	0.077599	0.62	1.307860	2.31	0.12224	2.23	1137	12	849	27	743	31	65
S10 S_2.1_10-25-55	25	382	37	0.063415	0.61	0.997329	2.05	0.11406	1.95	722	13	702	21	696	26	96
S10 S_3.1_10-25-55	25	687	52	0.067563	1.38	0.851736	4.24	0.09143	4.01	855	29	626	40	564	43	66
S10 S_4.1_10-25-55	25	215	33	0.073490	0.58	1.768238	2.11	0.17451	2.03	1027	12	1034	28	1037	39	101
S10 S_5.1_10-25-55	25	1328	172	0.074902	0.73	1.575857	1.88	0.15259	1.74	1066	15	961	24	915	30	86
S10 S_6.1_10-25-55	25	411	63	0.073127	0.62	1.810898	1.76	0.17960	1.65	1017	13	1049	23	1065	32	105
S10 S_7.1_10-25-55	25	3252	121	0.123776	1.25	0.708929	3.34	0.04154	3.09	2011	22	544	28	262	16	13
S10 S_8.1_10-25-55	25	1468	393	0.125244	0.64	5.042121	1.91	0.29198	1.80	2032	11	1826	33	1651	52	81
S10 S_8.2_10-25-55	25	611	213	0.129270	0.61	6.781080	1.93	0.38045	1.83	2088	11	2083	34	2078	65	100
S10 S_9.1_10-25-55	25	432	68	0.072965	0.57	1.854578	1.88	0.18434	1.79	1013	12	1065	25	1091	36	108
S10 S_10.1_10-25-55	25	254	23	0.061148	0.65	0.931817	1.81	0.11052	1.68	644	14	669	18	676	22	105
S10 S_10.2_10-25-55	25	115	11	0.061634	0.69	0.935554	1.80	0.11009	1.66	661	15	671	18	673	21	102
S10 S_11.1_10-25-55	25	726	68	0.061017	0.58	0.930760	1.69	0.11063	1.59	640	12	668	17	676	20	106
S10 S_11.2_10-25-55	25	345	35	0.064390	1.13	1.041561	1.96	0.11732	1.60	754	24	725	20	715	22	95
S10 S_12.1_10-25-55	25	900	86	0.062873	1.07	0.966889	1.96	0.11153	1.65	704	23	687	20	682	21	97
S10 S_13.1_10-25-55	25	245	25	0.062538	0.73	1.011906	1.95	0.11735	1.81	693	16	710	20	715	25	103
S10 S_13.2_10-20-55	20	197	20	0.109656	5.32	1.673722	5.97	0.11070	2.71	1794	97	999	77	677	35	38
S10 S_13.3_10-20-55	20	148	17	0.144426	1.05	2.472503	3.44	0.12416	3.28	2281	18	1264	50	754	47	33
S10 S_14.1_10-25-55	25	1098	97	0.083662	0.74	1.179860	1.82	0.10228	1.66	1285	14	791	20	628	20	49
S10 S_14.2_10-25-55	25	1178	106	0.083602	0.85	1.302320	6.60	0.11298	6.55	1283	17	847	77	690	86	54
S10 S_15.1_10-25-55	25	2195	91	0.092630	4.14	0.611942	6.91	0.04791	5.54	1480	78	485	54	302	33	20
S10 S_16.1_10-25-55	25	217	20	0.060884	0.65	0.919799	1.96	0.10957	1.85	635	14	662	19	670	24	106
S10 S_17.1_10-25-55	25	983	72	0.068889	2.10	0.844468	4.58	0.08891	4.07	895	43	622	43	549	43	61
S10 S_18.1_10-25-55	25	626	89	0.072618	0.64	1.647216	2.04	0.16452	1.93	1003	13	988	26	982	35	98
S10 S_19.1_10-25-55	25	405	31	0.087143	4.28	1.036429	5.27	0.08626	3.08	1364	82	722	55	533	32	39
S10 S_20.1_10-25-55	25	1233	111	0.062056	0.81	0.893284	1.86	0.10440	1.68	676	17	648	18	640	20	95
S10 S_21.1_10-25-55	25	177	28	0.073464	0.71	1.857454	1.84	0.18337	1.70	1027	14	1066	24	1085	34	106
S10 S_22.1_10-25-55	25	172	18	0.064096	0.88	1.049461	2.28	0.11875	2.10	745	19	729	24	723	29	97
S10 S_23.1_10-25-55	25	477	47	0.062681	0.62	1.001469	1.88	0.11588	1.77	697	13	705	19	707	24	101
S10 S_23.2_10-25-55	25	562	55	0.064192	0.80	0.985258	1.87	0.11132	1.69	748	17	696	19	680	22	91
S10 S_24.1_10-25-55	25	401	38	0.061341	0.61	0.941076	1.79	0.11127	1.69	651	13	673	18	680	22	104

Table 5

sample	spot Ø	U [ppm]	Pb [ppm]	ratios $^{207}Pb/^{206}Pb$	1σ	$^{207}Pb/^{235}U$	1σ	$^{206}Pb/^{238}U$	1σ	$^{207}Pb/^{206}Pb$	2σ	$^{207}Pb/^{235}U$	2σ	$^{206}Pb/^{238}U$	2σ	conc.
S8 L_1.1_10-35-55	35	731	63	0.062131	0.30	0.882789	0.83	0.10305	0.78	679	6	642	8	632	9	93
S8 L_1.2_10-35-55	35	308	28	0.060269	0.67	0.875916	1.94	0.10541	1.82	613	14	639	18	646	22	105
S8 L_2.1_10-35-55	35	955	129	0.080402	0.63	1.778234	2.15	0.16041	2.06	1207	12	1038	28	959	37	79
S8 L_3.1_10-35-55	35	272	25	0.065632	0.86	1.005293	1.60	0.11109	1.35	795	18	706	16	679	17	85
S8 L_4.1_10-35-55	35	353	64	0.120373	0.39	3.342706	0.83	0.20140	0.74	1962	7	1491	13	1183	16	60
S8 L_4.2_10-25-55	25	509	202	0.161342	0.58	9.542483	3.13	0.42896	3.07	2470	10	2392	58	2301	120	93
S8 L_5.1_10-35-55	35	314	27	0.062969	0.40	0.885584	1.01	0.10200	0.93	707	8	644	10	626	11	89
S8 L_6.1_10-35-55	35	321	28	0.064164	0.47	0.897184	1.21	0.10141	1.12	747	10	650	12	623	13	83
S8 L_7.1_10-35-55	35	224	32	0.072794	0.40	1.673689	0.88	0.16675	0.78	1008	8	999	11	994	14	99
S8 L_8.1_10-35-55	35	181	64	0.130352	0.29	6.938641	1.05	0.38606	1.01	2103	5	2104	19	2105	36	100
S8 L_9.1_10-35-55	35	525	71	0.069021	0.28	1.471451	0.89	0.15462	0.84	899	6	919	11	927	15	103
S8 L_10.1_10-35-55	35	119	11	0.060762	0.34	0.866531	1.20	0.10343	1.15	631	7	634	11	634	14	101
S8 L_11.1_10-25-55	25	216	19	0.060244	0.72	0.857201	1.76	0.10320	1.61	612	16	629	17	633	19	103
S8 L_12.1_10-25-55	25	249	24	0.061554	0.63	0.945108	1.89	0.11136	1.78	659	14	676	19	681	23	103
S8 L_13.1_10-25-55	25	451	41	0.064369	0.81	0.944863	2.36	0.10646	2.22	754	17	675	23	652	28	87
S8 L_14.1_10-25-55	25	1721	77	0.090818	2.27	0.688446	6.84	0.05498	6.45	1443	43	532	57	345	43	24
S8 L_15.1_10-25-55	25	231	20	0.059324	0.65	0.833028	2.21	0.10184	2.11	579	14	615	20	625	25	108
S8 L_16.1_10-25-55	25	768	93	0.083269	1.28	1.678712	4.90	0.14621	4.73	1276	25	1000	63	880	78	69
S8 L_16.2_10-25-55	25	1496	104	0.089042	1.45	1.066583	6.30	0.08688	6.13	1405	28	737	67	537	63	38
S8 L_17.1_10-25-55	25	164	15	0.061290	0.65	0.888874	1.82	0.10518	1.70	649	14	646	17	645	21	99
S8 L_107.1_10-35-55	35	450	53	0.072019	0.68	1.339644	1.91	0.13491	1.78	986	14	863	22	816	27	83
S8 L_18.1_10-35-55	35	837	72	0.072242	0.79	0.996260	2.01	0.10002	1.85	993	16	702	20	615	22	62
S8 L_19.1_10-35-55	35	100	10	0.073592	1.98	1.098952	2.59	0.10830	1.67	1030	40	753	28	663	21	64
S8 L_20.1_10-35-55	35	82	8	0.071990	2.56	1.060979	3.13	0.10689	1.80	986	52	734	33	655	22	66
S8 L_21.1_10-35-55	35	599	51	0.061037	0.76	0.826210	1.82	0.09817	1.66	641	16	612	17	604	19	94
S8 L_22.1_10-35-55	35	239	22	0.061822	0.67	0.895715	1.71	0.10508	1.57	668	14	649	16	644	19	96
S8 L_23.1_10-35-55	35	787	77	0.079767	0.59	1.222759	1.76	0.11118	1.65	1191	12	811	20	680	21	57
S8 L_24.1_10-35-55	35	308	45	0.071891	0.61	1.654017	1.73	0.16687	1.62	983	12	991	22	995	30	101
S8 L_25.1_10-35-55	35	316	33	0.093328	4.85	1.504712	5.15	0.11693	1.73	1495	92	932	64	713	23	48
S8 L_26.1_10-35-55	35	522	39	0.068184	2.41	0.825132	4.41	0.08777	3.69	874	50	611	41	542	38	62
S8 L_27.1_10-35-55	35	251	22	0.060531	0.70	0.856346	1.81	0.10260	1.68	623	15	628	17	630	20	101
S8 L_28.1_10-35-55	35	140	15	0.065624	0.77	1.092754	1.76	0.12077	1.58	794	16	750	19	735	22	93
S8 L_29.1_10-35-55	35	401	29	0.067829	0.86	0.764344	3.16	0.08173	3.04	863	18	577	28	506	30	59
S8 L_30.1_10-35-55	35	645	42	0.074644	1.95	0.762653	2.99	0.07410	2.27	1059	39	576	26	461	20	44
S8 S_1.1_10-25-55	25	227	19	0.060622	0.60	0.835128	1.60	0.09991	1.48	626	13	616	15	614	17	98
S8 S_2.1_10-25-55	25	879	51	0.072128	0.63	0.684402	2.36	0.06882	2.27	990	13	529	20	429	19	43
S8 S_3.1_10-25-55	25	431	106	0.121372	0.64	4.630761	1.75	0.27671	1.63	1976	11	1755	29	1575	46	80
S8 S_4.1_10-25-55	25	159	22	0.072275	0.59	1.653470	1.56	0.16592	1.44	994	12	991	20	990	26	100
S8 S_5.1_10-25-55	25	1070	71	0.085696	5.04	0.930227	5.55	0.07873	2.32	1331	98	668	55	489	22	37
S8 S_6.1_10-25-55	25	963	189	0.125981	0.62	4.049742	5.72	0.23314	5.68	2043	11	1644	95	1351	139	66
S8 S_7.1_10-25-55	25	635	68	0.079441	0.85	1.391955	2.62	0.12708	2.48	1183	17	886	31	771	36	65
S8 S_8.1_10-25-55	25	438	57	0.070980	0.69	1.490233	1.64	0.15227	1.49	957	14	926	20	914	25	95
S8 S_9.1_10-25-55	25	3112	112	0.101990	0.90	0.573965	2.32	0.04082	2.14	1661	17	461	17	258	11	16
S8 S_9.2_10-15-55	15	1087	128	0.077588	3.00	1.539294	4.23	0.14389	2.97	1136	60	946	53	867	48	76
S8 S_10.1_10-25-55	25	782	87	0.075327	0.65	1.344778	1.63	0.12948	1.50	1077	13	865	19	785	22	73
S8 S_11.1_10-25-55	25	314	40	0.070580	0.61	1.428753	1.60	0.14682	1.48	945	12	901	19	883	24	93
S8 S_12.1_10-25-55	25	814	60	0.065359	0.90	0.775091	1.86	0.08601	1.63	786	19	583	17	532	17	68
S8 S_13.1_10-25-55	25	305	26	0.062963	0.87	0.872620	1.64	0.10052	1.40	707	18	637	16	617	16	87
S8 S_14.1_10-25-55	25	789	73	0.062687	0.72	0.945276	1.87	0.10937	1.73	698	15	676	19	669	22	96
S8 S_15.1_10-25-55	25	716	91	0.073712	0.75	1.513933	1.99	0.14896	1.84	1034	15	936	24	895	31	87
S8 S_16.1_10-25-55	25	188	20	0.068033	0.70	1.179764	1.95	0.12577	1.81	870	15	791	21	764	26	88
S8 S_17.1_10-25-55	25	196	18	0.062193	0.73	0.930300	1.72	0.10849	1.56	681	16	668	17	664	20	98
S8 S_18.1_10-25-55	25	622	66	0.080118	3.41	1.346519	4.24	0.12189	2.53	1200	67	866	50	741	36	62
S8 S_19.1_10-25-55	25	46	5	0.073197	1.71	1.209594	2.64	0.11985	2.00	1019	35	805	30	730	28	72
S8 S_20.1_10-20-55	20	429	38	0.061621	0.66	0.883360	2.03	0.10397	1.93	661	14	643	19	638	23	96
S8 S_21.1_10-25-55	20	924	67	0.068055	0.82	0.792204	1.95	0.08443	1.77	870	17	592	18	522	18	60
S8 S_21.2_10-20-55	20	365	34	0.061893	0.76	0.902427	2.13	0.10575	1.99	670	16	653	21	648	25	97
S8 S_22.1_10-20-55	20	278	90	0.119734	0.60	6.092328	1.78	0.36903	1.68	1952	11	1989	31	2025	58	104
S8 S_23.1_10-20-55	20	291	42	0.085556	2.39	1.968137	6.10	0.16684	5.61	1328	46	1105	84	995	104	75
S8 S_24.1_10-20-55	20	156	21	0.076693	0.98	1.598027	2.61	0.15112	2.42	1113	20	969	33	907	41	81
S8 S_25.1_10-20-55	20	306	46	0.074724	0.65	1.796955	2.04	0.17441	1.93	1061	13	1044	27	1036	37	98
S8 S_26.1_10-20-55	20	222	19	0.061334	0.70	0.842129	1.79	0.09958	1.64	651	15	620	17	612	19	94
S8 S_27.1_10-20-55	20	265	25	0.063415	0.96	0.934459	2.27	0.10687	2.06	722	20	670	22	655	26	91
S8 S_28.1_10-20-55	20	430	51	0.077857	0.74	1.441718	2.01	0.13430	1.87	1143	15	906	24	812	29	71

Table 6

	spot	U	Pb	ratios												
sample	Ø	[ppm]	[ppm]	$^{207}Pb/^{206}Pb$	1σ	$^{207}Pb/^{235}U$	1σ	$^{206}Pb/^{238}U$	1σ	$^{207}Pb/^{206}Pb$	2σ	$^{207}Pb/^{235}U$	2σ	$^{206}Pb/^{238}U$	2σ	conc.
D600L_1.1_10-35-55	35	432	45	0.063356	0.67	1.071062	1.97	0.12261	1.86	720	14	739	21	746	26	104
D600L_2.1_10-35-55	35	172	23	0.069609	0.68	1.499854	2.00	0.15627	1.88	917	14	930	25	936	33	102
D600L_3.1_10-35-55	35	1333	282	0.176065	0.70	5.477466	2.95	0.22563	2.87	2616	12	1897	51	1312	68	50
D600L_3.2_10-35-55	35	2010	251	0.192177	1.41	3.581073	5.86	0.13515	5.68	2761	23	1545	95	817	88	30
D600L_4.1_10-35-55	35	504	219	0.170895	0.66	10.862712	2.11	0.46101	2.00	2566	11	2511	40	2444	82	95
D600L_5.1_10-35-55	35	165	16	0.075871	0.97	1.135610	2.34	0.10856	2.13	1092	19	770	25	664	27	61
D600L_5.2_10-25-55	25	69	17	0.146236	0.99	5.359337	3.84	0.26580	3.71	2302	17	1878	67	1519	101	66
D600L_6.1_10-35-55	35	118	10	0.061297	0.75	0.831656	2.07	0.09840	1.93	650	16	615	19	605	22	93
D600L_7.1_10-35-55	35	381	159	0.169525	0.68	10.353507	2.07	0.44295	1.95	2553	11	2467	39	2364	77	93
D600L_8.1_10-35-55	35	563	38	0.072828	1.77	0.780527	2.62	0.07773	1.94	1009	36	586	23	483	18	48
D600L_8.2_10-35-55	35	220	16	0.057607	0.67	0.667750	2.01	0.08407	1.90	515	15	519	16	520	19	101
D600L_9.1_10-35-55	35	160	20	0.068824	0.94	1.383568	2.33	0.14580	2.13	893	19	882	28	877	35	98
D600L_9.2_10-35-55	35	258	30	0.066976	0.99	1.243338	2.87	0.13464	2.70	837	21	820	33	814	41	97
D600L_10.1_10-35-55	35	705	56	0.058945	0.68	0.753522	2.00	0.09271	1.89	565	15	570	18	572	21	101
D600L_11.1_10-35-55	35	141	60	0.162296	0.68	10.091272	2.36	0.45096	2.26	2480	12	2443	44	2400	91	97
D600L_12.1_10-35-55	35	79	11	0.072603	0.76	1.604500	2.13	0.16028	1.98	1003	15	972	27	958	35	96
D600L_13.1_10-35-55	35	155	22	0.071601	0.70	1.633895	2.09	0.16550	1.97	975	14	983	26	987	36	101
D600L_14.1_10-35-55	35	131	10	0.060500	0.74	0.738092	2.09	0.08848	1.96	621	16	561	18	547	21	88
D600L_15.1_10-35-55	35	279	51	0.077787	0.69	2.244404	2.10	0.20926	1.99	1141	14	1195	30	1225	44	107
D600L_16.1_10-35-55	35	371	37	0.062226	0.68	0.990845	2.05	0.11549	1.93	682	15	699	21	705	26	103
D600L_17.1_10-35-55	35	112	9	0.060875	0.77	0.826335	2.07	0.09845	1.93	635	17	612	19	605	22	95
D600L_18.1_10-35-55	35	158	38	0.096000	0.68	3.671162	2.02	0.27735	1.90	1548	13	1565	32	1578	53	102
D600L_19.1_10-35-55	35	206	29	0.072277	0.70	1.616419	2.06	0.16220	1.94	994	14	977	26	969	35	98
D600L_20.1_10-35-55	35	49	7	0.072628	0.80	1.696586	2.15	0.16942	2.00	1004	16	1007	28	1009	37	101
D600L_21.1_10-35-55	35	238	82	0.128279	0.67	6.665042	2.04	0.37683	1.93	2075	12	2068	36	2061	68	99
D600L_22.1_10-35-55	35	378	32	0.059960	0.68	0.812024	2.01	0.09822	1.89	602	15	604	18	604	22	100
D600L_23.1_10-35-55	35	255	36	0.070986	0.68	1.611140	2.01	0.16461	1.90	957	14	975	25	982	35	103
D600L_24.1_10-35-55	35	121	14	0.066573	0.73	1.286607	2.04	0.14017	1.90	824	15	840	23	846	30	103
D600L_25.1_10-35-55	35	903	246	0.170331	0.67	6.720672	2.63	0.28617	2.55	2561	11	2075	47	1622	73	63
D600L_25.2_10-25-55	25	621	182	0.170493	0.69	7.336132	2.29	0.31208	2.19	2562	12	2153	41	1751	67	68
D600L_26.1_10-35-55	35	58	9	0.071668	0.74	1.622780	2.30	0.16422	2.18	977	15	979	29	980	40	100
D600L_27.1_10-35-55	35	394	36	0.061159	0.73	0.903714	2.01	0.10717	1.87	645	16	654	19	656	23	102
D600L_28.1_10-35-55	35	189	59	0.113879	0.68	5.409246	2.05	0.34450	1.93	1862	12	1886	35	1908	64	102
D600L_29.1_10-35-55	35	124	18	0.071687	0.70	1.672801	2.02	0.16924	1.89	977	14	998	26	1008	35	103
D600L_30.1_10-35-55	35	42	5	0.068763	0.77	1.310032	2.17	0.13817	2.03	892	16	850	25	834	32	94
D600L_31.1_10-35-55	35	239	21	0.060395	0.70	0.862927	2.11	0.10363	1.99	618	15	632	20	636	24	103
D600L_32.1_10-35-55	35	165	17	0.063767	0.71	1.073296	2.02	0.12207	1.89	734	15	740	21	742	27	101
D600L_33.1_10-35-55	35	538	52	0.063977	0.70	0.992117	2.02	0.11247	1.89	741	15	700	20	687	25	93
D600L_34.1_10-35-55	35	39	5	0.070503	0.75	1.492314	2.27	0.15351	2.14	943	15	927	28	921	37	98
D600L_35.1_10-35-55	35	155	51	0.121007	0.69	6.048741	2.06	0.36254	1.94	1971	12	1983	36	1994	67	101
D600L_36.1_10-35-55	35	282	87	0.120523	0.75	5.606095	2.07	0.33736	1.94	1964	13	1917	36	1874	63	95
D600L_37.1_10-35-55	35	452	39	0.066444	0.75	0.926006	2.04	0.10108	1.89	820	16	666	20	621	22	76
D600L_38.1_10-35-55	35	346	33	0.062049	0.68	0.958028	2.07	0.11198	1.95	676	14	682	21	684	25	101
D600L_39.1_10-35-55	35	227	20	0.064897	1.02	0.927240	2.40	0.10363	2.17	771	21	666	24	636	26	82
D600L_40.1_10-35-55	35	190	28	0.071270	0.68	1.654477	1.98	0.16837	1.86	965	14	991	25	1003	35	104
D600L_41.1_10-35-55	35	113	17	0.073039	0.71	1.709448	2.00	0.16975	1.87	1015	14	1012	26	1011	35	100
D600L_42.1_10-35-55	35	297	29	0.061539	0.70	0.958440	2.03	0.11296	1.90	658	15	682	20	690	25	105
D600L_43.1_10-35-55	35	36	5	0.070072	0.91	1.512198	2.43	0.15652	2.25	930	19	935	30	937	39	101
D600L_44.1_10-35-55	35	361	52	0.071534	0.70	1.637329	2.03	0.16601	1.91	973	14	985	26	990	35	102
D600L_45.1_10-35-55	35	422	56	0.073413	0.72	1.538270	2.09	0.15197	1.97	1025	15	946	26	912	33	89
D600L_46.1_10-35-55	35	213	21	0.062652	0.72	1.002483	2.06	0.11605	1.93	696	15	705	21	708	26	102
D600L_47.1_10-35-55	35	252	120	0.175004	0.67	12.033431	2.05	0.49870	1.94	2606	11	2607	39	2608	84	100
D600L_47.2_10-25-55	25	176	83	0.176107	0.68	11.751471	2.13	0.48397	2.02	2617	11	2585	40	2545	85	97
D600L_48.1_10-35-55	35	382	37	0.064258	0.80	0.995220	2.06	0.11233	1.90	750	17	701	21	686	25	91
D600L_49.1_10-35-55	35	78	7	0.060186	0.87	0.824436	2.36	0.09935	2.19	610	19	611	22	611	26	100
D600S_1.1_10-35-55	35	80	7	0.065103	1.57	0.870263	2.05	0.09695	1.31	778	33	636	19	597	15	77
D600S_2.1_10-35-55	35	60	9	0.072736	1.19	1.644987	1.78	0.16402	1.32	1007	24	988	23	979	24	97
D600S_3.1_10-35-55	35	1036	102	0.109449	2.81	1.630456	4.33	0.10804	3.30	1790	51	982	55	661	41	37
D600S_4.1_10-35-55	35	863	106	0.066893	0.95	1.290250	1.54	0.13989	1.21	834	20	841	18	844	19	101
D600S_5.1_10-35-55	35	232	24	0.063944	1.04	1.039300	1.90	0.11788	1.59	740	22	724	20	718	22	97
D600S_6.1_10-35-55	35	49	4	0.064953	1.42	0.848632	1.93	0.09476	1.30	773	30	624	18	584	15	76
D600S_7.1_10-35-55	35	122	11	0.062772	1.05	0.920504	1.67	0.10635	1.30	701	22	663	16	652	16	93
D600S_8.1_10-35-55	35	83	12	0.074684	1.00	1.694545	1.95	0.16456	1.68	1060	20	1006	25	982	31	93
D600S_9.1_10-35-55	35	841	219	0.136747	1.04	5.075744	2.25	0.26920	1.99	2186	18	1832	38	1537	55	70
D600S_10.1_10-35-55	35	223	105	0.177499	0.94	11.729531	1.58	0.47927	1.27	2630	16	2583	30	2524	53	96
D600S_11.1_10-35-55	35	291	109	0.134220	0.94	7.276731	1.54	0.39320	1.23	2154	16	2146	28	2138	45	99
D600S_12.1_10-35-55	35	407	117	0.188973	0.98	7.530111	1.91	0.28900	1.64	2733	16	2177	35	1637	48	60
D600S_13.1_10-35-55	35	412	188	0.161640	0.95	10.476488	1.56	0.47007	1.24	2473	16	2478	29	2484	51	100
D600S_14.1_10-35-55	35	557	51	0.076439	2.29	1.068216	2.97	0.10135	1.89	1107	46	738	31	622	22	56
D600S_15.2_10-35-55	35	264	23	0.064439	2.22	0.892203	2.60	0.10042	1.36	756	47	648	25	617	16	82
D600S_16.1_10-35-55	35	251	37	0.073095	0.97	1.625589	1.59	0.16129	1.26	1017	20	980	20	964	23	95
D600S_17.1_10-35-55	35	361	163	0.176194	0.95	10.677604	1.98	0.43952	1.73	2617	16	2495	37	2349	68	90

Table 7

sample	spot Ø	U [ppm]	Pb [ppm]	ratios $^{207}Pb/^{206}Pb$	1σ	$^{207}Pb/^{235}U$	1σ	$^{206}Pb/^{238}U$	1σ	$^{207}Pb/^{206}Pb$	2σ	$^{207}Pb/^{235}U$	2σ	$^{206}Pb/^{238}U$	2σ	conc.
D470L_1.1_10-35-55	35	69	10	0.074645	1.52	1.676141	1.70	0.16286	0.76	1059	31	1000	22	973	14	92
D470L_2.1_10-35-55	35	110	11	0.064408	1.25	1.034282	1.53	0.11647	0.88	755	26	721	16	710	12	94
D470L_3.1_10-35-55	35	193	17	0.061740	1.20	0.891279	1.42	0.10470	0.76	665	26	647	14	642	9	97
D470L_4.1_10-35-55	35	132	38	0.109322	1.18	4.793333	1.50	0.31800	0.92	1788	22	1784	25	1780	29	100
D470L_5.1_10-35-55	35	298	24	0.059941	1.22	0.773851	1.55	0.09363	0.96	601	26	582	14	577	11	96
D470L_6.1_10-35-55	35	175	17	0.063249	1.20	0.994829	1.41	0.11408	0.74	717	25	701	14	696	10	97
D470L_8.1_10-35-55	35	355	67	0.083116	1.18	2.467578	1.38	0.21532	0.72	1272	23	1263	20	1257	17	99
D470L_9.1_10-35-55	35	168	15	0.077424	1.73	1.075048	1.94	0.10070	0.88	1132	34	741	21	619	10	55
D470L_10.1_10-35-55	35	63	6	0.063110	1.41	0.950408	1.69	0.10922	0.94	712	30	678	17	668	12	94
D470L_11.1_10-35-55	35	119	18	0.071908	1.24	1.694605	1.43	0.17092	0.73	983	25	1007	18	1017	14	103
D470L_12.1_10-35-55	35	91	8	0.061668	1.34	0.839793	1.54	0.09877	0.76	663	29	619	14	607	9	92
D470L_13.1_10-35-55	35	185	18	0.063250	1.32	0.966748	1.52	0.11085	0.75	717	28	687	15	678	10	95
D470L_14.1_10-35-55	35	89	8	0.064214	2.34	0.895174	2.50	0.10111	0.91	749	49	649	24	621	11	83
D470L_15.1_10-35-55	35	58	5	0.060362	1.40	0.780138	1.59	0.09374	0.76	617	30	586	14	578	8	94
D470L_16.1_10-35-55	35	49	4	0.061430	1.58	0.783012	1.75	0.09245	0.75	654	34	587	16	570	8	87
D470L_17.2_10-25-55	25	63	2	0.051011	5.57	0.266404	5.73	0.03788	1.37	241	128	240	25	240	6	99
D470L_18.1_10-35-55	35	516	41	0.058301	0.95	0.756842	1.53	0.09415	1.20	541	21	572	13	580	13	107
D470L_19.1_10-35-55	35	920	88	0.062573	0.97	0.988991	1.62	0.11463	1.30	694	21	698	16	700	17	101
D470L_20.1_10-35-55	35	590	22	0.052825	1.11	0.330436	1.63	0.04537	1.19	321	25	290	8	286	7	89
D470L_21.1_10-35-55	35	132	44	0.120527	0.93	6.245480	1.62	0.37582	1.32	1964	17	2011	28	2057	47	105
D470L_22.1_10-35-55	35	464	38	0.058651	0.94	0.793745	1.56	0.09815	1.24	554	21	593	14	604	14	109
D470L_23.1_10-35-55	35	148	12	0.061570	1.07	0.835682	1.69	0.09844	1.31	659	23	617	16	605	15	92
D470L_24.1_10-35-55	35	387	35	0.060115	1.00	0.903274	1.63	0.10898	1.29	608	22	653	16	667	16	110
D470L_25.1_10-35-55	35	667	69	0.063409	0.94	1.074665	1.63	0.12292	1.33	722	20	741	17	747	19	104
D470L_26.1_10-35-55	35	278	23	0.058601	1.02	0.805872	1.61	0.09974	1.25	552	22	600	15	613	15	111
D470L_27.1_10-35-55	35	252	37	0.071664	0.95	1.704956	1.75	0.17255	1.47	976	19	1010	23	1026	28	105
D470L_28.1_10-35-55	35	108	10	0.062111	1.07	0.908769	1.68	0.10612	1.30	678	23	656	16	650	16	96
D470L_29.1_10-35-55	35	155	16	0.063496	0.96	1.080800	1.77	0.12345	1.49	725	20	744	19	750	21	104
D470L_30.1_10-35-55	35	372	34	0.081658	1.13	1.194011	1.74	0.10605	1.32	1237	22	798	19	650	16	53
D470L_31.1_10-35-55	35	204	26	0.068513	0.94	1.409045	1.55	0.14916	1.23	884	19	893	18	896	21	101
D470L_32.1_10-35-55	35	1881	327	0.174933	0.94	4.418893	1.79	0.18321	1.52	2605	16	1716	30	1084	30	42
D470L_32.2_10-35-55	35	1905	340	0.169889	0.94	4.440462	1.88	0.18957	1.63	2557	16	1720	31	1119	34	44
D470L_33.1_10-35-55	35	75	11	0.069328	1.04	1.612438	1.68	0.16868	1.32	909	21	975	21	1005	25	111
D470L_34.1_10-35-55	35	121	20	0.075988	0.98	2.019754	1.58	0.19277	1.23	1095	20	1122	22	1136	26	104
D470L_35.1_10-35-55	35	187	63	0.121210	0.94	6.221460	1.57	0.37227	1.26	1974	17	2007	28	2040	44	103
D470L_36.1_10-35-55	35	503	46	0.061647	0.96	0.895812	1.53	0.10539	1.20	662	21	649	15	646	15	98
D470L_37.1_10-35-55	35	20	2	0.079614	2.44	1.325250	2.73	0.12073	1.23	1187	48	857	32	735	17	62
D470L_38.1_10-35-55	35	240	24	0.064847	0.96	1.043370	1.56	0.11669	1.23	769	20	726	16	712	17	92
D470L_39.1_10-35-55	35	1690	257	0.181116	1.24	4.012798	5.85	0.16069	5.72	2663	21	1637	97	961	103	36
D470L_40.1_10-35-55	35	1138	311	0.181336	0.95	7.160021	2.84	0.28637	2.68	2665	16	2132	51	1623	77	61
D470L_41.1_10-35-55	35	357	129	0.128682	0.95	7.054161	1.59	0.39758	1.28	2080	17	2118	29	2158	47	104
D470L_42.1_10-35-55	35	187	21	0.065373	0.99	1.156266	1.57	0.12828	1.22	786	21	780	17	778	18	99
D470L_43.1_10-35-55	35	978	75	0.057786	0.95	0.708826	1.51	0.08896	1.18	522	21	544	13	549	12	105
D470L_43.2_10-25-55	25	898	76	0.058192	0.98	0.770530	1.57	0.09603	1.23	537	22	580	14	591	14	110
D470L_44.1_10-35-55	35	1184	204	0.171420	0.94	4.285241	1.82	0.18131	1.56	2572	16	1691	30	1074	31	42
D470L_45.1_10-25-55	25	152	22	0.073863	1.87	1.641557	2.34	0.16119	1.41	1038	38	986	30	963	25	93
D470L_46.1_10-25-55	25	240	27	0.064808	1.03	1.128800	1.67	0.12632	1.31	768	22	767	18	767	19	100
D470L_47.1_10-25-55	25	138	22	0.071613	1.06	1.778317	1.89	0.18010	1.56	975	22	1038	25	1068	31	109
D470L_48.1_10-25-55	25	804	94	0.105712	1.85	1.881514	3.12	0.12909	2.51	1727	34	1075	42	783	37	45
D470S_1.1_10-35-55	35	199	16	0.060223	1.12	0.788949	1.71	0.09501	1.29	612	24	591	15	585	14	96
D470S_2.1_10-35-55	35	803	58	0.100738	3.31	1.141343	3.63	0.08217	1.50	1638	61	773	40	509	15	31
D470S_2.2_10-35-55	35	667	51	0.106870	3.49	1.245052	3.68	0.08449	1.17	1747	64	821	42	523	12	30
D470S_3.1_10-35-55	35	264	23	0.063970	1.02	0.880216	1.40	0.09980	0.96	741	22	641	13	613	11	83
D470S_4.1_10-35-55	35	451	31	0.057567	0.97	0.644660	1.36	0.08122	0.96	513	21	505	11	503	9	98
D470S_5.1_10-35-55	35	1016	195	0.099926	1.04	2.912307	2.11	0.21138	1.83	1623	19	1385	32	1236	41	76
D470S_6.1_10-35-55	35	454	41	0.069831	2.08	1.020180	2.80	0.10596	1.88	923	43	714	29	649	23	70
D470S_7.1_10-35-55	35	767	63	0.082652	0.97	1.055514	1.44	0.09262	1.06	1261	19	732	15	571	12	45
D470S_8.1_10-35-55	35	197	17	0.063480	1.31	0.895607	1.68	0.10232	1.05	724	28	649	16	628	13	87
D470S_9.1_10-35-55	35	107	10	0.063200	1.44	0.912852	1.82	0.10476	1.11	715	31	659	18	642	14	90
D470S_10.1_10-35-55	35	1247	82	0.114484	1.27	1.140602	1.65	0.07226	1.05	1872	23	773	18	450	9	24
D470S_10.2_10-35-55	35	594	63	0.070738	1.00	1.173362	1.51	0.12030	1.14	950	20	788	17	732	16	77
D470S_11.1_10-35-55	35	1271	70	0.103083	2.87	0.883199	3.49	0.06214	1.98	1680	53	643	33	389	15	23
D470S_11.2_10-35-55	35	1406	70	0.129000	1.00	0.969227	1.44	0.05449	1.03	2084	18	688	14	342	7	16
D470S_12.1_10-35-55	35	415	41	0.072654	1.89	1.141115	2.43	0.11391	1.52	1004	38	773	26	695	20	69
D470S_13.1_10-35-55	35	247	21	0.062295	1.05	0.822429	1.45	0.09575	1.00	684	22	609	13	589	11	86
D470S_14.1_10-35-55	35	61	6	0.064918	1.12	0.980616	1.54	0.10956	1.06	772	24	694	16	670	13	87
D470S_15.1_10-35-55	35	494	36	0.086289	2.18	0.966949	2.52	0.08127	1.27	1345	42	687	25	504	12	37
D470S_16.1_10-35-55	35	86	10	0.065521	1.06	1.146754	1.42	0.12694	0.93	791	22	776	15	770	14	97
D470S_17.1_10-35-55	35	218	21	0.063764	1.20	0.967378	1.61	0.11003	1.06	734	26	687	16	673	14	92
D470S_18.1_10-35-55	35	34	3	0.087947	2.88	1.302839	3.16	0.10744	1.29	1381	55	847	37	658	16	48
D470S_19.1_10-35-55	35	129	13	0.064785	1.04	1.001412	1.51	0.11211	1.09	767	22	705	15	685	14	89
D470S_20.1_10-35-55	35	434	31	0.058413	0.98	0.670045	1.41	0.08319	1.01	545	21	521	12	515	10	94
D470S_21.1_10-35-55	35	82	8	0.063363	1.00	0.987594	1.54	0.11304	1.17	720	21	697	16	690	15	96
D470S_22.1_10-35-55	35	521	234	0.214800	1.08	14.014898	3.26	0.47321	3.08	2942	17	2751	63	2498	128	85
D470S_22.2_10-25-55	25	1065	163	0.186457	1.13	3.988161	1.87	0.15513	1.50	2711	19	1632	31	930	26	34
D470S_23.1_10-25-55	25	155	16	0.065966	1.09	1.035383	1.56	0.11384	1.12	805	23	722	16	695	15	86

Table 8

sample	spot Ø	U [ppm]	Pb [ppm]	ratios $^{207}Pb/^{206}Pb$	1σ	$^{207}Pb/^{235}U$	1σ	$^{206}Pb/^{238}U$	1σ	$^{207}Pb/^{206}Pb$	2σ	$^{207}Pb/^{235}U$	2σ	$^{206}Pb/^{238}U$	2σ	conc.
01WP19_10-35-50	35	199	16	0.06016	0.865929	0.78501	1.366175	0.09464	1.056693	609	37	588	12	583	12	96
02WP19_10-35-50	35	57	8	0.07360	0.863175	1.66703	1.311009	0.16427	0.98675	1030	35	996	17	980	18	95
03WP19_10-35-50	35	393	113	0.10840	0.803599	4.67879	1.181829	0.31304	0.866573	1773	29	1763	20	1756	27	99
04WP19_10-35-50	35	316	32	0.06326	0.813397	1.01048	1.19925	0.11586	0.881241	717	35	709	12	707	12	99
05WP19_10-35-50	35	434	36	0.06011	0.816779	0.80276	1.285921	0.09686	0.99321	607	35	598	12	596	11	98
06WP19_10-35-50	35	86	7	0.05978	0.866318	0.79055	1.434852	0.09592	1.143807	596	37	591	13	590	13	99
07WP19_10-35-50	35	84	7	0.05981	0.933839	0.79489	1.40474	0.09639	1.049399	597	40	594	13	593	12	99
08WP19_10-35-50	35	212	18	0.06150	0.831595	0.86558	1.239844	0.10208	0.9196	657	36	633	12	627	11	95
09WP19_10-35-50	35	329	110	0.12982	0.809438	6.50536	1.533368	0.36344	1.302316	2095	28	2047	27	1998	45	95
10WP19_10-35-50	35	526	31	0.05472	0.817479	0.51494	1.312	0.06826	1.026193	401	37	422	9	426	8	106
11WP19_10-35-50	35	986	94	0.06196	0.805689	0.93704	1.251943	0.10968	0.958241	673	35	671	12	671	12	100
12WP19_10-35-50	35	153	46	0.11373	0.806939	5.31475	1.325618	0.33892	1.05172	1860	29	1871	23	1881	34	101
13WP19_10-35-50	35	266	27	0.06318	0.826036	1.02368	1.203103	0.11751	0.874713	714	35	716	12	716	12	100
14WP19_10-35-50	35	167	24	0.07286	0.850017	1.66158	1.345499	0.16539	1.042994	1010	34	994	17	987	19	98
15WP19_10-35-50	35	478	13	0.05138	0.857846	0.22792	1.378792	0.03217	1.07943	258	39	208	5	204	4	79
16WP19_10-35-50	35	561	43	0.05912	0.814965	0.71797	1.292567	0.08807	1.003275	572	35	549	11	544	10	95
16bWP19_10-35-50	35	638	49	0.05876	0.821614	0.73680	1.273838	0.09095	0.973455	558	36	561	11	561	10	101
17WP19_10-35-50	35	135	20	0.07246	0.816963	1.68599	1.438828	0.16876	1.184398	999	33	1003	18	1005	22	101
18WP19_10-25-50	25	697	68	0.12500	0.807802	1.74112	1.724183	0.10102	1.523241	2029	29	1024	22	620	18	31
19WP19_10-35-50	35	52	8	0.07338	0.832473	1.74050	1.642493	0.17203	1.4159	1024	34	1024	21	1023	26	100
20WP19_10-35-50	35	209	81	0.13879	0.802581	7.92868	1.429283	0.41432	1.182672	2212	28	2223	26	2235	45	101
21WP19_10-35-50	35	204	31	0.07373	0.816387	1.73175	1.391995	0.17035	1.127459	1034	33	1020	18	1014	21	98
22WP19_10-35-50	35	225	19	0.06022	0.820485	0.79858	1.419086	0.09618	1.157847	612	35	596	13	592	13	97
23WP19_10-35-50	35	734	58	0.06477	0.841961	0.81205	1.970996	0.09094	1.782113	767	35	604	18	561	19	73
24WP19_10-25-50	25	268	124	0.18046	0.802319	11.75646	1.407563	0.47250	1.156511	2657	27	2585	27	2495	48	94
25WP19_10-35-50	35	265	41	0.09372	0.911798	2.23339	1.511539	0.17283	1.205559	1503	34	1192	21	1028	23	68
26WP19_10-35-50	35	188	29	0.07408	0.813637	1.79318	1.405279	0.17556	1.145777	1044	33	1043	18	1043	22	100
27WP19_10-35-50	35	125	13	0.06617	0.974778	1.16559	1.562145	0.12775	1.220698	812	41	785	17	775	18	95
28WP19_10-35-50	35	194	63	0.12155	0.801961	6.05768	1.464222	0.36145	1.225073	1979	29	1984	26	1989	42	101
29WP19_10-35-50	35	234	75	0.12510	0.835172	5.99801	1.583318	0.34775	1.345134	2030	30	1976	28	1924	45	95
30WP19_10-35-50	35	168	68	0.17546	0.801571	10.31199	1.416244	0.42625	1.167575	2610	27	2463	26	2289	45	88
31WP19_10-35-50	35	53	30	0.24191	0.920201	18.18887	1.861566	0.54533	1.618227	3133	29	3000	36	2806	74	90
32WP19_10-35-50	35	231	21	0.06120	0.811635	0.88555	1.526611	0.10494	1.292977	646	35	644	15	643	16	100
33WP19_10-35-50	35	182	28	0.07364	0.825524	1.73396	1.586966	0.17077	1.355349	1032	33	1021	21	1016	26	99
34WP19_10-35-50	35	168	13	0.05838	0.850932	0.70624	1.670208	0.08774	1.437188	544	37	543	14	542	15	100
35WP19_10-35-50	35	184	88	0.17715	0.801989	12.10053	1.58936	0.49542	1.372181	2626	27	2612	30	2594	59	99
36WP19_10-50-50	50	20	2	0.06752	0.906452	1.14685	1.518602	0.12320	1.2184	854	38	776	16	749	17	88
37WP19_10-35-50	35	22	3	0.07378	0.948847	1.74314	1.670343	0.17136	1.374677	1035	38	1025	21	1020	25	98
38WP19_10-35-50	35	242	29	0.06741	0.810343	1.29514	1.747786	0.13934	1.54858	851	34	844	20	841	24	99
39WP19_10-35-50	35	197	16	0.05975	0.833398	0.79772	1.601839	0.09683	1.367968	594	36	596	14	596	15	100
40WP19_10-35-50	35	766	66	0.06036	0.805777	0.83231	1.486036	0.10001	1.24861	616	35	615	14	614	15	100
41WP19_10-35-50	35	177	26	0.07359	0.811426	1.71513	1.70167	0.16904	1.49575	1030	33	1014	22	1007	28	98
42WP19_10-35-50	35	100	9	0.06060	0.852781	0.85439	1.60595	0.10226	1.360823	625	37	627	15	628	16	100
43WP19_10-50-50	50	80	10	0.06979	0.824765	1.44290	1.622053	0.14994	1.396717	922	34	907	20	901	24	98
44WP19_10-35-50	35	156	13	0.05977	0.86716	0.79793	1.602479	0.09682	1.34758	595	38	596	14	596	15	100
45WP19_10-35-50	35	132	11	0.06993	1.595722	0.98992	2.075339	0.10267	1.326916	926	65	699	21	630	16	68
46WP19_10-35-50	35	232	33	0.07169	0.817325	1.60229	1.330857	0.16211	1.050314	977	33	971	17	968	19	99
47WP19_10-35-50	35	34	10	0.10802	0.821148	4.67806	1.451443	0.31411	1.19683	1766	30	1763	24	1761	37	100
48WP19_10-50-50	50	57	4	0.06083	0.823742	0.76664	1.297642	0.09141	1.002659	633	35	578	11	564	11	89
49WP19_10-50-50	50	54	8	0.07403	0.828683	1.79937	1.330364	0.17629	1.040746	1042	33	1045	17	1047	20	100
50WP19_10-35-50	35	185	16	0.06019	0.848397	0.80836	1.392829	0.09741	1.104624	610	37	602	13	599	13	98
51WP19_10-20-50	20	370	158	0.17397	0.804633	10.46297	1.369002	0.43620	1.107579	2596	27	2477	26	2334	43	90
52WP19_10-25-50	25	170	73	0.17394	0.809937	10.61159	1.254716	0.44247	0.958287	2596	27	2490	23	2362	38	91
53WP19_10-50-50	50	207	29	0.07189	0.803139	1.63618	1.172923	0.16507	0.85482	983	33	984	15	985	16	100
54WP19_10-35-50	35	176	25	0.07155	0.807583	1.61777	1.387327	0.16398	1.128046	973	33	977	17	979	21	101
55WP19_10-35-50	35	119	40	0.13122	0.814389	6.71565	1.607758	0.37117	1.386239	2114	29	2075	29	2035	48	96
56WP19_10-75-50	35	142	22	0.12371	7.479892	2.93663	7.700259	0.17217	1.82899	2010	265	1391	120	1024	35	51
57WP19_10-35-50	35	170	24	0.07104	0.814846	1.57559	1.19895	0.16085	0.879492	959	33	961	15	961	16	100
58WP19_10-35-50	50	28	2	0.06116	0.936561	0.82964	1.353106	0.09838	0.976601	645	40	613	12	605	11	94
59WP19_10-35-50	35	474	12	0.05013	0.829301	0.20857	1.35392	0.03018	1.070215	201	38	192	5	192	4	95
59bWP19_10-35-50	35	312	8	0.05034	0.853064	0.21212	1.333046	0.03056	1.02435	211	39	195	5	194	4	92
60WP19_10-35-50	35	34	5	0.07317	0.903702	1.71763	1.384856	0.17026	1.049356	1019	37	1015	18	1014	19	100
61WP19_10-35-50	35	410	142	0.12536	0.805764	6.43468	1.317229	0.37228	1.042035	2034	29	2037	23	2040	37	100
62WP19_10-35-50	50	56	8	0.07999	1.014293	1.84577	1.381359	0.16736	0.937743	1197	40	1062	18	998	17	83
63WP19_10-35-50	35	890	70	0.05914	0.921093	0.74810	1.263474	0.09174	0.864843	572	40	567	11	566	9	99
64WP19_10-35-50	35	101	9	0.06062	0.859201	0.89912	1.276932	0.10757	0.944631	626	37	651	12	659	12	105

Table 9

sample	spot Ø	U [ppm]	Pb [ppm]	ratios $^{207}Pb/^{206}Pb$	1σ	$^{207}Pb/^{235}U$	1σ	$^{206}Pb/^{238}U$	1σ	$^{207}Pb/^{206}Pb$	2σ	$^{207}Pb/^{235}U$	2σ	$^{206}Pb/^{238}U$	2σ	conc.
01WP103sm_10-35-50	35	63	34	0.20007	0.81	14.97042	1.22	0.54268	0.91	2827	26	2813	23	2795	41	99
02WP103sm_10-35-50	35	594	52	0.06042	0.81	0.83539	1.27	0.10028	0.99	619	35	617	12	616	12	100
03WP103sm_10-35-50	35	221	72	0.12113	0.81	5.93093	1.31	0.35510	1.04	1973	29	1966	23	1959	35	99
04WP103sm_10-35-50	35	514	54	0.06378	0.81	1.05971	1.42	0.12050	1.17	734	34	734	15	733	16	100
05WP103sm_10-35-50	35	254	39	0.07462	0.81	1.83428	1.30	0.17827	1.02	1058	33	1058	17	1058	20	100
06WP103sm_10-35-50	35	118	60	0.18654	0.81	13.64560	1.30	0.53054	1.02	2712	27	2725	25	2744	46	101
07WP103sm_10-35-50	35	337	33	0.06289	0.81	0.98926	1.36	0.11409	1.09	704	35	698	14	696	14	99
08bWP103sm_10-25-50	25	63	32	0.19859	0.82	14.41919	1.35	0.52660	1.07	2815	27	2778	26	2727	47	97
09WP103sm_10-35-50	35	570	51	0.06157	0.81	0.90457	1.20	0.10656	0.89	659	35	654	12	653	11	99
10WP103sm_10-35-50	35	419	32	0.05871	0.82	0.72896	1.24	0.09004	0.93	557	36	556	11	556	10	100
11WP103sm_10-35-50	35	142	62	0.16343	0.81	10.42338	1.30	0.46257	1.02	2491	27	2473	24	2451	42	98
12WP103sm_10-35-50	35	126	63	0.18619	0.80	13.55225	1.43	0.52790	1.19	2709	27	2719	27	2733	53	101
13WP103sm_10-35-50	35	55	28	0.18700	0.81	13.50589	1.28	0.52382	0.99	2716	27	2716	24	2715	44	100
14bWP103sm_10-35-50	35	152	49	0.14327	2.84	6.39227	6.39	0.32360	5.73	2267	98	2031	115	1807	182	80
14WP103sm_10-35-50	35	309	147	0.17415	0.80	11.73734	1.32	0.48880	1.05	2598	27	2584	25	2565	45	99
15WP103sm_10-35-50	35	376	35	0.06148	0.81	0.90836	1.29	0.10716	1.01	656	35	656	13	656	13	100
16WP103sm_10-35-50	35	95	49	0.18683	0.80	13.53936	1.33	0.52560	1.06	2714	27	2718	25	2723	47	100
17bWP103sm_10-35-50	35	131	5	0.05416	0.92	0.35586	1.33	0.04766	0.96	378	41	309	7	300	5	79
17cWP103sm_10-35-50	35	114	5	0.05509	0.93	0.36288	1.39	0.04778	1.03	416	41	314	7	301	6	72
17dWP103sm_10-75-50	75	98	4	0.05538	0.81	0.37329	1.26	0.04889	0.96	427	36	322	7	308	6	72
17eWP103sm_10-75-50	75	118	5	0.05491	0.88	0.36353	1.27	0.04802	0.92	409	39	315	7	302	5	74
17WP103sm_10-50-50	50	67	3	0.05514	1.00	0.36915	1.36	0.04856	0.92	418	44	319	7	306	5	73
18WP103sm_10-35-50	35	90	41	0.16996	0.85	11.29713	1.37	0.48207	1.08	2557	29	2548	26	2536	45	99
19WP103sm_10-35-50	35	123	39	0.12189	0.80	6.13563	1.29	0.36508	1.01	1984	29	1995	23	2006	35	101
20WP103sm_10-35-50	35	133	67	0.18686	0.80	13.71868	1.27	0.53248	0.98	2715	26	2730	24	2752	44	101
21WP103sm_10-35-50	35	89	44	0.18794	0.81	13.66140	1.46	0.52719	1.22	2724	27	2727	28	2730	54	100
22WP103sm_10-35-50	35	74	37	0.18708	0.81	13.54329	1.25	0.52504	0.95	2717	27	2718	24	2721	42	100
23bWP103sm_10-25-50	25	247	131	0.18794	0.81	13.86411	1.33	0.53503	1.06	2724	27	2740	25	2763	48	101
23WP103sm_10-25-50	25	388	203	0.18824	0.80	13.61932	1.28	0.52474	1.00	2727	26	2724	24	2719	45	100
24bWP103sm_10-50-50	50	32	16	0.18605	0.80	13.81621	1.27	0.53860	0.98	2708	27	2737	24	2778	44	103
24WP103sm_10-35-50	35	174	89	0.18668	0.80	13.47529	1.37	0.52352	1.11	2713	26	2714	26	2714	49	100
25WP103sm_10-35-50	35	59	30	0.18738	0.81	13.60240	1.31	0.52649	1.03	2719	27	2722	25	2727	46	100
26WP103sm_10-35-50	35	49	25	0.19892	0.82	14.60648	1.49	0.53256	1.24	2817	27	2790	28	2752	55	98
27WP103sm_10-35-50	35	174	17	0.06224	0.82	0.95558	1.37	0.11135	1.09	682	35	681	14	681	14	100
28WP103sm_10-50-50	50	32	12	0.13950	0.81	8.06304	1.42	0.41919	1.17	2221	28	2238	26	2257	45	102
29WP103sm_10-50-50	50	111	59	0.19867	0.80	14.84285	1.31	0.54185	1.04	2815	26	2805	25	2791	48	99
30WP103sm_10-35-50	35	141	75	0.20408	0.80	15.43298	1.25	0.54847	0.96	2859	26	2842	24	2819	44	99
31WP103L_10-50-50	50	38	19	0.18573	0.80	13.57669	1.36	0.53017	1.09	2705	26	2721	26	2742	49	101
32WP103L_10-75-50	75	70	5	0.06451	1.44	0.78070	1.72	0.08777	0.95	759	61	586	15	542	10	71
33bWP103L_10-25-50	25	165	73	0.17369	0.80	11.01570	1.26	0.45997	0.96	2594	27	2524	24	2439	39	94
33WP103L_10-75-50	35	68	30	0.16784	0.83	10.71807	1.46	0.46314	1.21	2536	28	2499	27	2453	49	97
34WP103L_10-35-50	35	137	44	0.12125	0.81	6.02265	1.28	0.36025	0.99	1975	29	1979	22	1983	34	100
35WP103L_10-25-50	25	74	39	0.19877	0.81	14.93828	1.23	0.54507	0.93	2816	27	2811	24	2805	42	100
36WP103L_10-50-50	50	18	9	0.18757	0.81	13.78757	1.29	0.53312	1.01	2721	27	2735	25	2755	45	101
37WP103L_10-50-50	50	24	13	0.19637	0.80	14.85374	1.26	0.54862	0.97	2796	26	2806	24	2819	44	101
38WP103L_10-50-50	50	21	8	0.13451	0.81	7.38867	1.30	0.39839	1.02	2158	28	2160	23	2162	38	100
39bWP103L_10-75-50	75	22	0	0.07473	1.30	0.22464	1.64	0.02180	0.99	1061	52	206	6	139	3	13
39cWP103L_10-100-50	100	20	0	0.07279	1.13	0.21460	1.45	0.02138	0.90	1008	46	197	5	136	2	14
39dWP103L_10-120-50	120	16	0	0.07187	1.11	0.20991	1.37	0.02118	0.81	982	45	193	5	135	2	14
39eWP103L_10-120-60	0	0	0	0.07521	1.27	0.22598	1.46	0.02179	0.73	1074	51	207	5	139	2	13
39fWP103L_10-120-70	0	0	0	0.07488	1.08	0.22734	1.29	0.02202	0.72	1065	43	208	5	140	2	13
39WP103L_10-50-50	50	20	0	0.07623	2.12	0.22591	2.31	0.02149	0.90	1101	85	207	9	137	2	12
40bWP103L_10-100-50	100	92	2	0.05527	0.89	0.16120	1.25	0.02115	0.88	423	40	152	4	135	2	32
40cWP103L_10-120-50	120	48	1	0.05821	0.92	0.16929	1.22	0.02109	0.79	538	40	159	4	135	2	25
40dWP103L_10-75-50	75	100	2	0.05518	0.89	0.16267	1.27	0.02138	0.91	420	40	153	4	136	2	32
40eWP103L_10-75-50	75	84	1	0.05626	0.94	0.16660	1.25	0.02148	0.81	463	42	156	4	137	2	30
40WP103L_10-50-50	50	90	2	0.05453	0.94	0.15765	1.41	0.02097	1.05	393	42	149	4	134	3	34
41WP103L_10-35-50	35	358	25	0.05797	0.82	0.65841	1.29	0.08237	1.00	529	36	514	10	510	10	96
42WP103L_10-35-50	35	198	64	0.12094	0.81	5.98419	1.51	0.35886	1.27	1970	29	1974	26	1977	43	100
43WP103L_10-50-50	50	78	6	0.05833	0.85	0.69017	1.39	0.08581	1.10	542	37	533	11	531	11	98
44WP103L_10-25-50	25	69	34	0.18723	0.82	13.12967	1.23	0.50861	0.92	2718	27	2689	23	2651	40	98
45WP103L_10-50-50	50	204	8	0.05305	0.84	0.35069	1.34	0.04795	1.05	331	38	305	7	302	6	91
46bWP103L_10-35-50	35	155	57	0.13388	0.81	7.40759	1.31	0.40128	1.04	2150	28	2162	24	2175	38	101
46WP103L_10-25-50	25	58	23	0.14550	0.85	8.52840	1.31	0.42511	1.00	2294	29	2289	24	2284	38	100
47WP103L_10-50-50	50	57	29	0.18731	0.80	13.69790	1.24	0.53039	0.94	2719	26	2729	24	2743	43	101
48WP103sm_10-35-50	35	65	37	0.21689	0.80	17.42037	1.22	0.58254	0.91	2958	26	2958	23	2959	43	100
49WP103sm_10-35-50	35	209	116	0.20950	0.80	16.28272	1.26	0.56369	0.98	2902	26	2894	24	2882	46	99
50WP103sm_10-35-50	35	117	67	0.21350	0.80	17.03627	1.28	0.57872	0.99	2932	26	2937	25	2944	47	100
51WP103sm_10-35-50	35	390	200	0.18576	0.80	13.56395	1.31	0.52958	1.03	2705	26	2720	25	2740	47	101
52WP103sm_10-35-50	35	197	110	0.21518	0.80	17.18238	1.46	0.57914	1.22	2945	26	2945	28	2945	58	100
53WP103sm_10-35-50	35	135	43	0.12092	0.81	5.96534	1.29	0.35780	1.00	1970	29	1971	23	1972	34	100
54WP103sm_10-50-50	50	17	9	0.20733	0.81	16.27294	1.37	0.56926	1.10	2885	26	2893	26	2905	52	101